Using isotopic and chronologic data to fingerprint strata: Challenges and benefits of variable sources to tectonic interpretations, the Paro Formation, Bhutan Himalaya

T. Tobgay,[1] S. Long,[1] N. McQuarrie,[1] M. N. Ducea,[2] and G. Gehrels[2]

Received 3 December 2009; revised 26 August 2010; accepted 15 September 2010; published 31 December 2010.

[1] We combine detrital zircons (DZ) and epsilon neodymium (ε_{Nd}) signatures with field mapping in the Paro Formation in western Bhutan. DZ age spectra are strongly variable and display signatures that have been used to uniquely identify both Greater Himalayan (GH) and Lesser Himalayan (LH) strata. DZ age peaks from six quartzite samples require sources for ~0.5, 0.8, 1.2, 1.4, 1.7, 1.8, and 2.5 Ga zircons in the Paro Formation. The youngest (~0.5 Ga) zircons argue for a Cambrian maximum deposition age. Two samples have a youngest 1.8 Ga peak typically attributed to Paleoproterozoic LH rocks. A ~450 Ma crystallization age from two granite samples constrains the minimum deposition age as Ordovician. New ε_{Nd} signatures from six detrital samples from the Paro Formation show significant variation with lithology. Schists have $\varepsilon_{Nd}(0)$ values between −12.0 and −16.9, while quartzite values vary between −18.8 and −24.5. These data imply that the Paro Formation was derived from both young and old sources, with DZ and ε_{Nd} values obtained from the same quartzite samples requiring old detritus while the ε_{Nd} values obtained from interbedded schist require younger detritus. Using published isotopic and chronologic definitions of Himalayan strata, schist-rich layers would be considered GH, while the interbedded quartzite would be LH. Thus, the Paro Formation refutes the generally accepted notion that different Himalayan tectonostratigraphic zones have unique DZ and ε_{Nd} signatures. Our data recommend caution in the use of DZ and ε_{Nd} signatures for tectonic interpretation, especially when making correlations with studies that extend 1000s of km along strike. **Citation:** Tobgay, T., S. Long, N. McQuarrie, M. N. Ducea, and G. Gehrels (2010), Using isotopic and chronologic data to fingerprint strata: Challenges and benefits of variable sources to tectonic interpretations, the Paro Formation, Bhutan Himalaya, *Tectonics*, *29*, TC6023, doi:10.1029/2009TC002637.

[1]Department of Geosciences, Princeton University, Princeton, New Jersey, USA.
[2]Department of Geosciences, University of Arizona, Tucson, Arizona, USA.

0278-7407/10/2009TC002637

1. Introduction

[2] The U-Pb ages of detrital zircons (DZ) from a sedimentary rock combined with whole-rock epsilon neodymium (ε_{Nd}) values provide a proxy for the age of formation of the original source materials that make up the sedimentary rock [*McCulloch and Wasserburg*, 1978; *McLennan et al.*, 1989; *Gehrels et al.*, 1999, 2000, 2006; *DeGraaff-Surpless et al.*, 2003; *Mapes*, 2009]. Studies that use geochemical tools for reconstructing the provenance of sedimentary rocks are based on the premise that the signature of measured DZ ages and whole-rock ε_{Nd} values provide records of identifiable provenance [*Gleason et al.*, 1994; *Sircombe*, 1999; *Dickinson and Gehrels*, 2003; *Sircombe and Hazelton*, 2004; *Barbeau et al.*, 2005]. In tectonic research, particularly in the Himalaya, geochemical signatures from DZ and/or ε_{Nd} of three lithotectonic units (Lesser, Greater, and Tethyan Himalaya) have been used to define stratigraphic horizons, help identify important geologic structures and determine unroofing histories [e.g., *Parrish and Hodges*, 1996; *Robinson et al.*, 2001; *DeCelles et al.*, 2004; *Martin et al.*, 2005; *Richards et al.*, 2005, 2006; *Imayama and Arita*, 2008; *Myrow et al.*, 2009, 2010]. Because these lithotectonic units record the early geologic history of the Himalayas and allow us to reconstruct their original depositional relationships, understanding the provenance and original geometry of the Lesser, Greater, and Tethyan Himalayan basins is critical for identifying and estimating the displacement magnitude along the major thrust sheets in the Himalayan orogen.

[3] Even though early DZ and isotopic analyses from the central Himalaya have been successfully applied to distinguish different Himalayan lithotectonic units, new data from the western Bhutan Himalaya indicate that the use of DZ and ε_{Nd} for fingerprinting formations is not straightforward. There are several potential hazards to this approach. First, depositional systems are sensitive to climatic and geologic factors, and sediment composition is subject to alteration by surface processes that occur during erosion, transportation, and after deposition [*Savage and Potter*, 1991; *Nesbitt and Young*, 1996; *Potter et al.*, 2001]. Second, DZs from a single sedimentary succession can have multiple sources with temporally varying influences, producing heterogeneity of age distributions, which can obscure provenance characterization [e.g., *Gehrels et al.*, 2000; *DeGraaff-Surpless et al.*, 2003; *Mapes*, 2009]. DZ signatures may reflect combined sources, complicating provenance determinations and the whole rock ε_{Nd} values

would, at best, reflect an average of contributing source components [*Gleason et al.*, 1994], but may be dominated by a source that is preferentially confined to shale horizons [*McLennan et al.*, 1989]. Third, sedimentary sorting, weathering of labile source rocks and diagenesis can affect Nd isotope ratios of coarse- and fine-grained components differently [*Frost and Winston*, 1987; *McLennan et al.*, 1989, 1990; *Awwiller and Mack*, 1989, *Ohr et al.*, 1991]. Thus, the combination of these factors suggests the need to understand the limitations of each technique prior to interpretation.

[4] Using U-Pb and isotopic techniques, *Parrish and Hodges* [1996] recognized important distinctions between Lesser Himalayan (LH) and Greater Himalayan (GH) rocks in the Annapurna region of the Nepal Himalaya. Based on the presence of 0.8–1.0 Ga (Neoproterozoic) zircons and less negative $\varepsilon_{Nd}(21)$ values in GH rocks, and the presence of >1.8 Ga (Paleoprotereozoic) zircons and more negative εNd(21) values in LH rocks, the authors were the first to suggest that GH and LH rocks were derived from different source areas. Since then, many studies have examined the DZ ages of GH and LH rocks and used differences in age spectra to define unique characteristics of different Himalayan strata [*Parrish and Hodges*, 1996; *DeCelles et al.*, 2000, 2004; *Gehrels et al.*, 2003; *Martin et al.*, 2005; *Yin*, 2006; *McQuarrie et al.*, 2008; *Myrow et al.*, 2009]. To a first order, $\varepsilon_{Nd}(0)$ values of LH and GH rocks support this distinction [e.g., *Parrish and Hodges*, 1996; *Whittington et al.*, 1999; *Ahmad et al.*, 2000; *DeCelles et al.*, 2004; *Martin et al.*, 2005; *Richards et al.*, 2005, 2006].

[5] Conclusions that have been drawn from U-Pb age spectra and ε_{Nd} values of rocks in northwest India and Nepal include the following: (1) GH are distinct from LH rocks based on DZ spectra and ε_{Nd} values [*Parrish and Hodges*, 1996; *Ahmad et al.*, 2000; *DeCelles et al.*, 2000, 2004; *Robinson et al.*, 2001; *Martin et al.*, 2005], (2) GH rocks did not receive detritus from India and thus were separated by some unknown distance from the Indian margin [*DeCelles et al.*, 2000; *Gehrels et al.*, 2003; *Martin et al.*, 2005], and (3) DZ spectra are relatively homogeneous within a given stratigraphic unit and the youngest zircons are generally (but not always) representative of the age of the strata [*Myrow et al.*, 2003, 2009; *DeCelles et al.*, 2004; *Martin et al.*, 2005; *Yin*, 2006; *Yin et al.*, 2010].

[6] In this paper, we present new U-Pb geochronologic and Nd isotopic data from the western Bhutan Himalaya, particularly from the Paro Formation. These data show strong variability in DZ spectra as well as $\varepsilon_{Nd}(0)$ values in schist and phyllite that are different (more positive) by 6–12 ε_{Nd} units than those of adjacent quartzite. The observed variations complicate the premise that specific detrital zircon signatures or ε_{Nd} values can uniquely define tectonostratigraphic packages in the Himalaya. This complication allows us to evaluate the benefits and limitations of such techniques for distinguishing strata, distinguishing variations in basin geometry from variations in provenance, and defining large-scale orogenic structures that have telescoped a margin with a long and varied deformation history.

2. Himalayan Geologic Background

[7] The Himalayan orogenic belt has been divided into four tectonostratographic zones, which are each bound by major structures that are continuous along strike across the majority of the orogen [*Heim and Gansser*, 1939; *Gansser*, 1964, 1983; *Le Fort*, 1975]. The tectonostratigraphic units and bounding structures, from south to north, are the Main Frontal Thrust (MFT), sub-Himalayan thrust system, Main Boundary Thrust (MBT), Lesser Himalayan (LH) zone, Main Central Thrust (MCT), Greater Himalayan (GH) zone, South Tibetan detachment (STD), and Tethyan Himalayan (TH) zone (Figure 1). The Himalayan tectonostratigraphic zones were originally defined with respect to significant changes in metamorphic grade [*Heim and Gansser*, 1939; *Gansser*, 1964]. Abrupt juxtaposition of higher-grade rocks over lower-grade rocks was used to define orogen-scale structures such as the MCT and MBT [*Heim and Gansser*, 1939; *Gansser*, 1964; *Le Fort*, 1975]. Thus to a first-order Himalayan tectonostratigraphy can be uniquely identified based solely on lithologic and/or petrologic characteristics. However, since LH, GH, and TH strata all contain similar protoliths, variations that include highly metamorphosed LH strata or less metamorphosed GH strata can lead to difficulties in uniquely identifying and correlating rocks [*Whittington et al.*, 1999; *Hodges*, 2000; *Argles et al.*, 2003; *Martin et al.*, 2005].

[8] Protoliths of metasedimentary rocks of the GH are largely Neoproterozoic in age [*Parrish and Hodges*, 1996; *DeCelles et al.*, 2000; *Gehrels et al.*, 2003; *Martin et al.*, 2005; *Yin*, 2006], and are separated from underlying LH rocks by the MCT. LH rocks represent a thick succession of clastic and carbonate rocks that blanketed the northern portion of the Indian craton during Proterozoic and Paleozoic time [*Upreti*, 1999; *Myrow et al.*, 2003; *Yin*, 2006; *Robinson et al.*, 2006; *McQuarrie et al.*, 2008]. In the Nepal Himalaya, LH rocks are proposed to be entirely of Paleoproterozoic and Mesoproterozoic age [*DeCelles et al.*, 2000; *Martin et al.*, 2005], although in northwestern India and Bhutan, LH rocks extend into the Cambrian [*Myrow et al.*, 2003; *Richards et al.*, 2005; *McQuarrie et al.*, 2008]. The TH zone, which lies structurally above the STD, represents a composite section including two superimposed rift to passive margin sequences. TH strata extend from Neoproterozoic to Cretaceous in age [*Gaetani and Garzanti*, 1991; *Brookfield*, 1993; *Garzanti*, 1999; *Yin*, 2006]. Recent work has shown temporal overlap between the TH and LH zones in the Cambrian, Ordovician, and in the Permian through Paleocene [*Myrow et al.*, 2003, 2009; *Yin*, 2006; *McQuarrie et al.*, 2008; *Long et al.*, 2010].

[9] DZ geochronology and isotopic studies have been widely used in many parts of the Himalaya to characterize and distinguish litho packages of LH, GH, and TH from one another [*Parrish and Hodges*, 1996; *Gehrels et al.*, 1999; *Whittington et al.*, 1999; *Ahmad et al.*, 2000; *DeCelles et al.*, 2000]. LH rocks had a sedimentary provenance that included a source of much older (>1.8 Ga) DZs [*DeCelles et al.*, 2000; *Parrish and Hodges*, 1996; *Robinson et al.*, 2001; *Martin et*

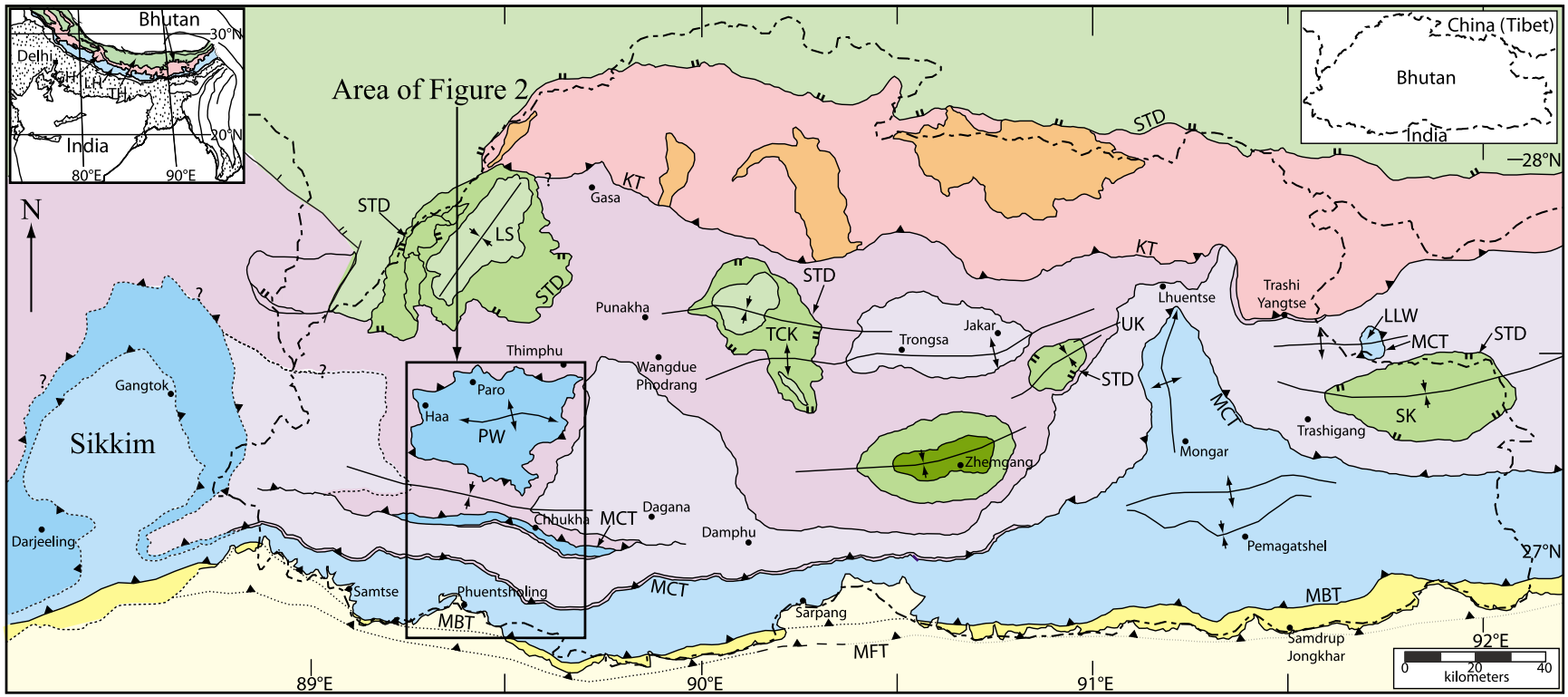

Figure 1. Simplified geologic map of Bhutan and surrounding region modified from *Long and McQuarrie* [2010]. Inset maps show the location and the international boundary of the Kingdom of Bhutan. Our study area (Figure 2) is shown by a rectangular box. Abbreviations: LH, Lesser Himalaya; GH, Greater Himalaya; TH, Tethyan Himalaya; STD, South Tibetan detachment; KT, Kakhtang Thrust; MCT, Main Central Thrust; MBT, Main Boundary Thrust; MFT, Main Frontal Thrust; LS, Lingshi Klippe; PW, Paro window; TCK, Tang Chu Klippe; UK, Ura Klippe; SK, Sakteng Klippe; LLW, Lum La window from *Yin et al.* [2010]. Map of Sikkim region is modified from *McQuarrie et al.* [2008]. Map projection: geographic lat/long (WGS84).

al., 2005; *Richards et al.*, 2005]. In contrast, GH rocks had a source containing generally younger DZs that range from 1.6 to 0.6 Ga [*Martin et al.*, 2005]. Similarly, the Tethyan sedimentary rocks have detrital zircons showing broad peaks at 1050 Ma and ~530 Ma [*Myrow et al.*, 2003, 2009; *DeCelles et al.*, 2004; *Martin et al.*, 2005] and may contain detrital zircons as young as 460 Ma [*Gehrels et al.*, 2003; *Long and McQuarrie*, 2010]. Nd isotopic signatures of Himalayan rocks follow a similar pattern where GH and TH rocks have an average $\varepsilon_{Nd}(0)$ value of −15 (less negative) while their Lesser Himalayan counterparts have an average value of −23 (more negative) [*DeCelles et al.*, 2000; *Robinson et al.*, 2001; *Martin et al.*, 2005; *Richards et al.*, 2005; *Imayama and Arita*, 2008].

3. Bhutan Tectonostratigraphy

[10] In Bhutan, the four Himalayan tectonostratigraphic zones are present (Figure 1). We describe these zones from south to north, along with their lithologic characteristics, DZ ages, and ε_{Nd} values in sections 3.1 to 3.5.

3.1. Sub-Himalayan Zone (Siwalik Group)

[11] The Siwalik Group represents synorogenic sediments deposited in the foreland basin of the Himalayan fold and thrust belt in mid-Miocene to Pliocene time [*Quade et al.*, 1995; *DeCelles et al.*, 1998, 2001]. In Bhutan, the Siwalik Group is exposed in discontinuous patches [*Gansser*, 1983; *Lakshminarayana and Singh*, 1995], with the missing sections either covered by Quaternary sediment, overridden by the MBT, or never deposited. In eastern Bhutan the Siwalik Group is up to ~5.5 km thick [*McQuarrie et al.*, 2008; *Long et al.*, 2010] (Figure 1). However, in southwestern Bhutan, near the town of Phuentsholing, the Siwaliks section is either absent or covered by Quaternary sediment (Figure 1).

3.2. Lesser Himalayan Zone

[12] LH strata above the MBT and below the MCT are composed of low-grade metasedimentary rocks, including quartzite, phyllite, and limestone [*Gansser*, 1983; *Bhargava*, 1995; *McQuarrie et al.*, 2008]. In western Bhutan, the LH section can be divided into three units. From old to young these are the Daling-Shumar Group, Baxa Group and the Jaishidanda Formation.

3.2.1. Daling-Shumar Group

[13] In Bhutan, the Daling-Shumar Group makes up the Paleoproterozoic LH section. In eastern Bhutan, the Daling-Shumar Group is separated into two distinct formations, the Daling Formation and the underlying Shumar Formation [*McQuarrie et al.*, 2008; *Long et al.*, 2010]. This two-part stratigraphy is also observed in western Bhutan.

[14] The Daling Formation consists of schist and phyllite with quartzite interbeds, and its lower contact is defined by the upsection transition from quartzite to phyllite and schist [*McQuarrie et al.*, 2008; *Long et al.*, 2010]. Also characteristic of the Daling Formation is the presence of bodies of mylonitized orthogneiss containing distinctive feldspar augen at different stratigraphic levels (Figure 2). The Shumar Formation consists of fine-grained quartzite, with medium to thick planar bedding [*Dasgupta*, 1995a; *McQuarrie et al.*, 2008; *Long et al.*, 2010]. Quartzite layers are often separated by cm- to m-scale interbeds of phyllite and schist. In western Bhutan (Figure 2), the Shumar Formation is ~2.6 km thick, and the combined thickness of Shumar and Daling formations is ~4.0 km.

[15] U-Pb ages of DZs from both the Daling and Shumar formations show strong peaks at ~1.9 Ga, however, the weighted mean age of the youngest three concordant zircons yield maximum deposition ages of 1865 ± 47 Ma, and 1816 ± 49 Ma [*Long et al.*, 2010]. Igneous rocks within the Daling Formation have crystallization ages of 1.78–1.9 Ga, 1.79–1.89 Ga and 1.76–1.84 Ga. [*Daniel et al.*, 2003; *Richards et al.*, 2006; *Long et al.*, 2010]. These data together suggest a deposition age between 1.8 and 1.9 Ga for the Daling-Shumar Group. Five samples from Daling-Shumar Group analyzed by *Richards et al.* [2006], have $\varepsilon_{Nd}(0)$ values of −27.0, −26.6, −27.3, −25.9, and −32.3. The Daling and Shumar formations have very negative ε_{Nd} values typical of old source terrane, which is consistent with the older DZ populations.

3.2.2. Baxa Group

[16] The Baxa Group is interpreted to stratigraphically overlie the Daling Formation in Bhutan [*Tangri*, 1995], and this contact is observed along strike in Sikkim [*Bhattacharyya and Mitra*, 2009]. In eastern Bhutan, the Baxa Group is primarily fine to medium grained, locally pebbly to conglomeratic quartzite, with jasper and rose quartz clasts [*McQuarrie et al.*, 2008; *Long et al.*, 2010]. However, the Baxa Group displays significant lateral variations in lithology. In western Bhutan, near Phuentsholing, the Baxa Group is divided into lower (Phuentsholing) and upper (Pangsari) formations [e.g., *Tangri*, 1995]. The Phuentsholing Formation consists of dark gray to black slate and phyllite with interbeds of limestone, creamy dolomite, and thin beds of fine- to medium-grained quartzite, while the Pangsari Formation consists of gray to green, locally talcose phyllite interbedded with red to pink marble and thin beds of fine- to medium-grained greenish quartzite.

[17] In eastern Bhutan, the Baxa Group yields DZ age spectra showing Cambrian (~520, 525 Ma) youngest peaks, with older peaks between 1.0 Ga and 1.7 Ga [*McQuarrie et al.*, 2008; *Long et al.*, 2010]. Phyllite samples collected within the Baxa Group in eastern Bhutan yielded $\varepsilon_{Nd}(0)$ value of −21 [*McQuarrie et al.*, 2008].

3.2.3. Jaishidanda Formation

[18] Beneath the MCT, a ~1.0 km thick interval of biotite-rich, locally garnet-bearing schist with interbeds of biotite-rich quartzite is present. These strata have been interpreted as part of the structurally overlying GH zone [*Jangpangi*, 1974;

Figure 2. Geologic map of part of the western Bhutan Himalaya showing detailed lithologic units in Paro Window. Strike and dip symbols indicate our mapping. Locations of DZ and ε_{Nd} samples are shown. Samples of *Richards et al.* [2006] are shown by asterisks (Bh10, Bh12, B85, and B88). Dashed line in Baxa Group represents boundary between Phuentsholing Formation and upper Pangsari Formation. Map projection: geographic lat/long (WGS84).

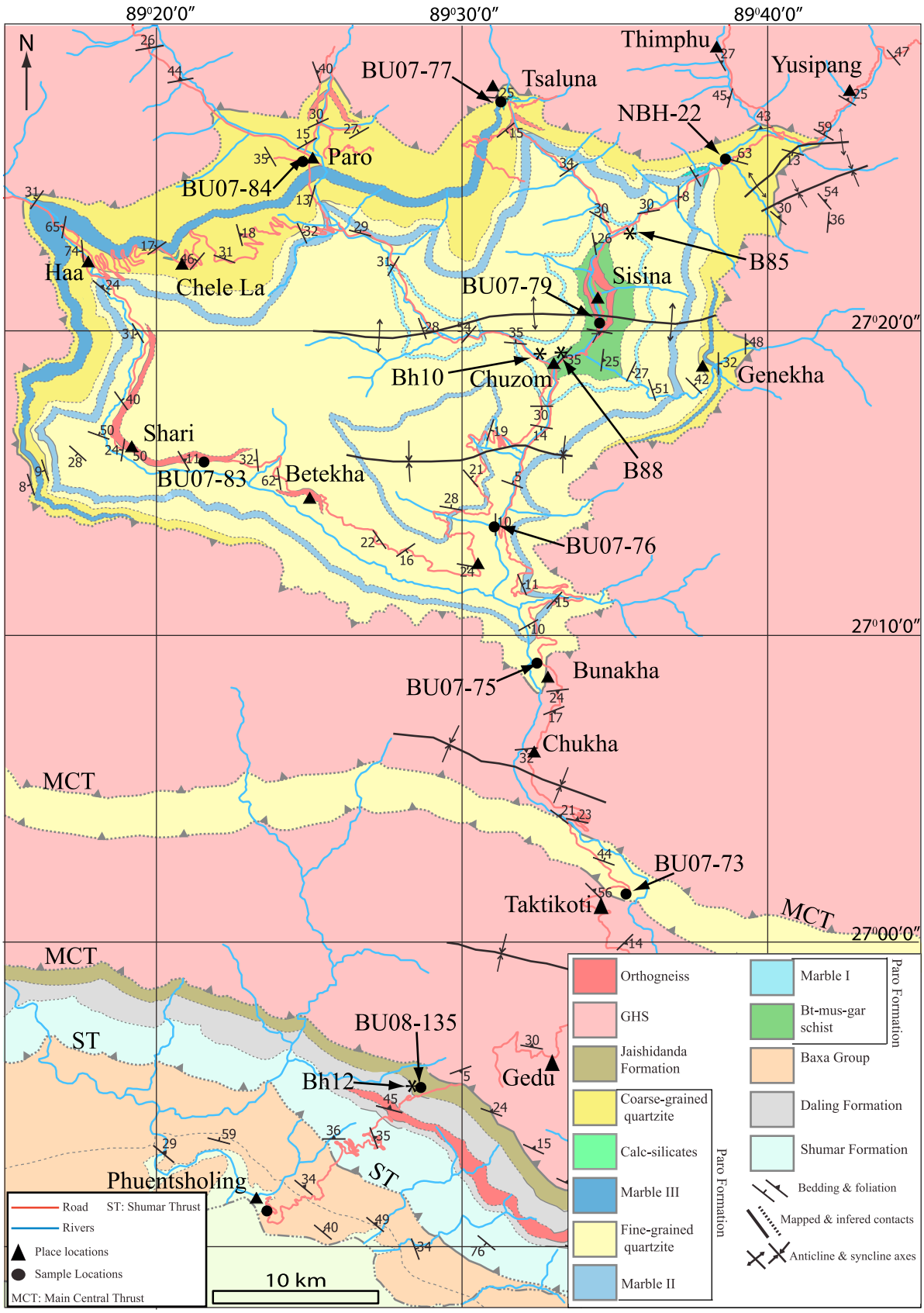
89°20′0″
89°30′0″
89°40′0″
N
Thimphu
Yusipang
BU07-77
Tsaluna
NBH-22
Paro
BU07-84
B85
Haa
Chele La
Sisina
BU07-79
27°20′0″
Bh10
Chuzom
Genekha
B88
Shari
BU07-83
Betekha
BU07-76
27°10′0″
Bunakha
BU07-75
Chukha
MCT
BU07-73
Taktikoti
MCT
27°00′0″
MCT
BU08-135
ST
Bh12
Gedu
Phuentsholing
ST
Road
Rivers
Place locations
Sample Locations
MCT: Main Central Thrust
ST: Shumar Thrust
10 km
Orthogneiss
GHS
Jaishidanda Formation
Coarse-grained quartzite
Calc-silicates
Marble III
Fine-grained quartzite
Marble II
Paro Formation
Marble I
Bt-mus-gar schist
Paro Formation
Baxa Group
Daling Formation
Shumar Formation
Bedding & foliation
Mapped & infered contacts
Anticline & syncline axes

Figure 2

Segupta and Raina, 1978; *Trichal and Jarayam*, 1989], as the uppermost part of the Daling-Shumar Group [*Guha Sarkar*, 1979; *Gansser*, 1983; *Ray et al.*, 1989], and as a unique lithotectonic unit called the Jaishidanda Formation (JF) mapped in thrust contact over the Daling-Shumar Group [*Dasgupta*, 1995b]. However, based on distinct lithologies and a lack of fault rocks at the base of the unit, *McQuarrie et al.* [2008] and *Long et al.* [2010] mapped the JF in depositional contact with the underlying Daling Formation. In western Bhutan, the JF contains biotite-rich, garnet-bearing schist with quartz vein boudins interbedded with light gray quartzite, with abundant crenulated, biotite-rich laminations and thin interbeds of biotite schist. The contact between the JF and the Daling Formation is distinguished by a downsection transition from gray, lithic clast-rich, and biotite-rich quartzite of the JF to clean, tan, thinly bedded quartzite containing rare biotite of the Daling Formation.

[19] DZs from the JF display peaks between ~475 Ma and 530 Ma, 0.9 Ga and 1.7 Ga, and a prominent peak at 2.5 Ga [*McQuarrie et al.*, 2008 and *Long et al.*, 2010]. This DZ age range, minus the young Ordovician to Cambrian peaks, is similar to the DZ data from strata immediately below the MCT in Arunachel Pradesh [*Yin*, 2006; *Yin et al.*, 2010]. The presence of DZ peaks as young as ~475 Ma indicates an Ordovician maximum deposition age.

3.3. Paro Formation

[20] The rocks of the Paro, Haa, Bunakha, and Thimphu regions (Figure 2) are referred to as the Paro Formation [*Jangpangi*, 1978a, 1978b, 1980; *Gansser*, 1983; *Dasgupta*, 1995b; *Ikemoto*, 2000; *Koike*, 2002]. The Paro Formation consists of high-grade metasedimentary and calcareous rocks, including calc-silicate rocks, marble, quartzite, quartz-garnet-staurolite-kyanite schist with subordinate feldspathic schist and bodies of two mica granite-composition orthogneiss [*Gansser*, 1983; *Dasgupta*, 1995b; *Ikemoto*, 2000]. Although the Paro Formation has been mapped in thrust contact with the overlying GH paragneiss [*Gansser*, 1983; *Dasgupta*, 1995b], the exact tectonic affinity of the unit is still ambiguous. *Jangpangi* [1978a, 1978b, 1980] correlated the upper quartzite-rich section and the lower carbonaceous section with the Shumar and Baxa formations of the LH sequence, respectively, based purely on lithology and lower metamorphic grade relative to the overlying GH rocks. Based on the presence of garnet- and staurolite-bearing muscovite-biotite schist, calc-silicate bands, and actinolite amphibolite lenses, *Gansser* [1983] designated upper greenschist to amphibolite facies for Paro Formation, and mapped the unit as a metasedimentary unit within the GH sequence. Later, *Dasgupta* [1995b] redesignated part of the Paro Formation as Jaishidanda Formation. *Richards et al.* [2006] analyzed three schist samples from the Paro Formation and reported less negative $\varepsilon_{Nd}(0)$ values (of −14.2, −16.4, and −16.9). Based on these values, *Richards et al.* [2006] mapped Paro rocks as part of the GH sequence. Our observations describing the complete stratigraphic section of the Paro Formation, along with detailed lithologic descriptions from our field mapping, are discussed in section 5.

3.4. Greater Himalaya

[21] In Bhutan, the GH section consists of orthogneiss and metasedimentary rocks that are separated from underlying LH rocks by the MCT [*Gansser*, 1983; *Golani*, 1995; *Grujic et al.*, 2002; *Long and McQuarrie*, 2010] (Figure 1). The GH rocks are intruded by both Miocene leucogranites related to the Himalayan orogenic event and Cambrian-Ordovician granites related to an older magmatic event [*Daniel et al.*, 2003; *Gehrels et al.*, 2003; *Richards et al.*, 2006; *Cawood et al.*, 2007]. The GH section is divided into a lower structural level above the MCT and below the Kakhtang Thrust (KT), and a higher structural level above the KT [*Grujic et al.*, 2002] (Figure 1). The lower structural level GH rocks overlie the Paro Formation. Here, GH rocks are paragneiss (muscovite-biotite-garnet-kyanite-fibrolite) interlayered with quartzite, both of which contain partial melt textures (cm-scale, granite-composition leucosomes, which are often deformed and sheared approximately concordant to primary foliation, and are generally distributed throughout the rock) (Figures 1 and 2). In the field, GH rocks can be differentiated from the Paro Formation based on the presence of partial melt textures and paragneiss indicating a distinct difference in metamorphic grade. This contrast in lithology, combined with pervasively sheared rocks present at the contact suggests that the GH is in thrust-sense shear zone contact above the Paro Formation.

[22] DZ age spectra from three quartzite samples in the metasedimentary unit of the structurally lower GH section yielded a Neoproterozoic (~900 Ma) youngest peak for one sample and Cambrian and Ordovician (500 and 460 Ma) youngest peaks for two samples [*Long and McQuarrie*, 2010]. An orthogneiss at the base of the GH section in eastern Bhutan yielded a 487 ± 7 U-Pb (zircon) crystallization age [*Long and McQuarrie*, 2010]. These data suggest an age range of Neoproterozoic to Ordovician for the GH metasedimentary unit in Bhutan [*Richards et al.*, 2006; *Long and McQuarrie*, 2010]. The lower and upper structural levels of the GH section have less negative average $\varepsilon_{Nd}(0)$ values of. −14.5 and −15.4, respectively [*Richards et al.*, 2006].

3.5. Tethyan Himalaya

[23] Throughout Bhutan, rocks of the TH zone are preserved above the GH section in synforms [*Gansser*, 1983; *Grujic et al.*, 2002; *Kellett et al.*, 2009]. The basal TH rocks, referred to as Chekha Formation, consist of quartzite, shale, siltstone, sandstone, and conglomeratic quartzite [*Tangri and Pande*, 1995]. These are overlain by Maneting Formation phyllite and fossiliferous limestone of Late Cambrian age locally known as Wachi La Formation [*Tangri and Pande*, 1995; *Hughes et al.*, 2010].

[24] Detrital zircon spectra of TH rocks from Bhutan all display peaks between 800 and 900 Ma [*McQuarrie et al.*, 2008; *Long and McQuarrie*, 2010; *Hughes et al.*, 2010]. In addition, samples from the Wachi La region (Deshichilling Formation and Quartzite Formation) in western Bhutan have a significant late Cambrian peak and unique late Cambrian fossils [*Hughes et al.*, 2010; *Myrow et al.*, 2010]. However, detrital zircon ages from the Chekha Formation in Central Bhutan (Zhemgang region) yield peaks as young as ~460 Ma,

which indicates an Ordovician or younger depositional age for TH rocks there [*Long and McQuarrie*, 2010]. No Nd isotope data exist for the TH rocks of Bhutan. However, based on the stratigraphic and structural position of TH rocks in relation to GH rocks along strike, similar, less negative ε_{Nd} values are expected.

4. Methods

4.1. Field Mapping

[25] Map data included in this paper come from our geologic mapping at 1:50,000 scale along roads and trails in western Bhutan (Figure 2). Mapping was focused on the Paro Formation although lithologic and structural data were also collected from LH and GH units between the MFT in the south to the MCT in the north. Our map data lie primarily in six transects (Figure 3a): (1) four from Chuzom to Bunakha, Paro, Tsaluna, and Genekha, (2) one along the road between Betekha and Chele La, and (3) one along the Phuentsholing-Thimphu highway between Chukha and Taktikoti. Our mapping was integrated with published geologic maps of Bhutan [*Gansser*, 1983; *Bhargava*, 1995; *Grujic et al.*, 2002] to help trace contacts along strike. The level of rock exposure in western Bhutan was good because of the fresh roadcuts.

4.2. U-Pb Geochronology

[26] DZ age populations reflect the age of the igneous or metamorphic protolith in which the zircon crystallized [*McCulloch and Wasserburg*, 1978; *McLennan et al.*, 1989]. The advent of high-precision analytical systems capable of producing high quality and quantity data sets necessary for provenance studies has revolutionized DZ geochronology and established it as a powerful tool for reconstructing the provenance of sedimentary rocks, particularly when primary depositional information has been erased by subsequent metamorphism [*Gehrels et al.*, 1999, 2000, 2006; *DeGraaff-Surpless et al.*, 2003; *Mapes*, 2009].

[27] U-Pb geochronologic analyses were conducted on individual zircon grains using laser-ablation multicollector inductively coupled plasma mass spectrometry (LA-MC-ICP-MS) at the University of Arizona LaserChron Center. See Text S1 (discussion 1) for a detailed discussion of the methodology of this laboratory.[1] Approximately 100 grains were dated per sample. We analyzed six detrital samples and two granite samples collected at different stratigraphic levels from the Paro Formation in order to provide age control on unit deposition, and to compare the isotopic variations. Sample locations and lithologies are listed in Table 1, and map locations are shown on Figure 2. The 505 U-Pb zircon analyses (after the removal of analyses with less than 70% concordance) are shown for each sample in Figure 3b in relative age probability plots (1σ errors), and data and measurement (analytical) errors (1σ) for individual analyses are listed in Data Set S1, and shown in Pb/U concordia plots for each sample in Figure S1.

[1]Auxiliary material data set is available at ftp://ftp.agu.org/apend/tc/2009TC002637. Other auxiliary material files are in the HTML.

[28] In general, $^{206}Pb^*/^{238}U$ (asterisk denotes correction for common Pb; see Text S1 (discussion 1) for details on this correction; all ages described in the text have had this correction) ratios were used for ages younger than ~1.0 Ga, and $^{207}Pb^*/^{206}Pb^*$ ratios were used for ages older than ~1.0 Ga, because this is the approximate crossover in precision for these two ages (Text S1, discussion 1). Age cutoffs used for each sample are listed in Table S1. Sources for systematic error, which include contributions from the fractionation correction, composition of common Pb, age of the calibration standard, and U decay constants (see footnotes of Data Set S1 for these values), are not added into the errors shown in Data Set S1 (which includes only measurement errors at 1σ), and could collectively shift age probability peaks by up to ~3% (2σ). Total systematic errors for each sample are listed at 2σ in Table S1 along with records of standards run for each individual sample. Note that the uncertainty of the weighted mean is based on the scatter and precision of the set of concordant ages, weighted according to their measurement errors. The systematic errors are then added to this measurement error quadratically to calculate the total error. Systematic errors include contributions from the fractionation correction, composition of common Pb, age of the calibration standard, and U decay constants.

4.3. Epsilon Neodymium Isotope Geochemistry

[29] Epsilon neodymium ε_{Nd} values give information on the age the source material since its extraction from the mantle [*McCulloch and Wasserburg*, 1978; *McLennan et al.*, 1989] and thus to a first order provide a proxy for the age of formation of the original source materials that make up the sedimentary rock. The utility of ε_{Nd} for provenance studies is founded on the coherent behavior of rare earth elements during sedimentary processes, and that sedimentary processes average the various sources from which the sediment was derived [*Boghossian et al.*, 1996].

[30] Nd isotopic ratios and the elemental concentrations of Sm and Nd were measured by thermal ionization mass spectrometry at the University of Arizona, following procedures reported by *Otamendi et al.* [2009]. Details on analytical errors and blanks specific to this study are reported in Text S1 (discussion 3). Analyses were done on six samples (five quartzite and one igneous) that were also analyzed for U-Pb ages. One additional sample came from a schist interbed close to a quartzite sample. Each sample is from a specific stratigraphic horizon, and reflects the ε_{Nd} value at that point. The seven samples analyzed span 3560 m of exposed Paro Formation section (from bottom to the top) (Figure 3a). Three samples represent lower, middle, and upper sections of the fine-grained quartzite unit that measures 1960 m thick. An igneous sample is from a 225 m thick orthogneiss body present in the midsection of fine-grained quartzite. One sample is from the upper stratigraphic level of a 1600 m thick coarse-grained quartzite. For each sample, the average of 100 isotopic ratios was taken to calculate the ε_{Nd} value. Analyzed samples have estimated analytical $\pm 2\sigma$ uncertainties of $^{147}Sm/^{144}Nd = 0.4\%$, and $^{143}Nd/^{144}Nd = 0.0012\%$, which corresponds to an ε_{Nd} error of ±0.5. Table 2 contains

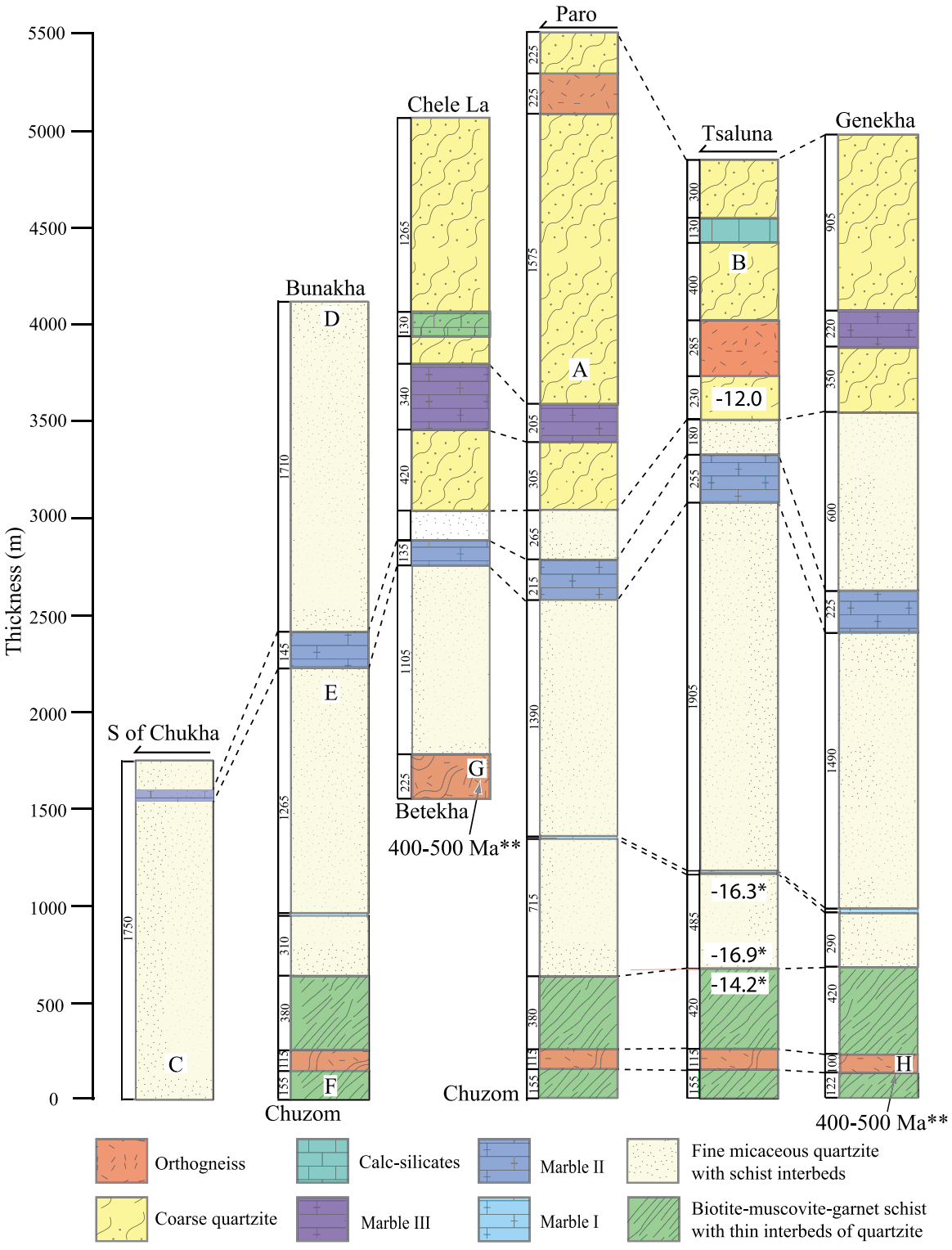

Figure 3a. Stratigraphic sections of the Paro Formation measured along different traverses (see Figure 2 for locations). Note thicknesses of units are in meters and the thickness of marble band I is ~10 m. The section has sample locations (labeled A–F) collected at different structural levels with their $\varepsilon_{Nd}(0)$ values next to it (A–F). The $\varepsilon_{Nd}(0)$ values marked with one asterisk are from *Richards et al.* [2006]. Two asterisks denote crystallization ages of orthogneiss samples (G = BU07-83 and H = BU08-128).

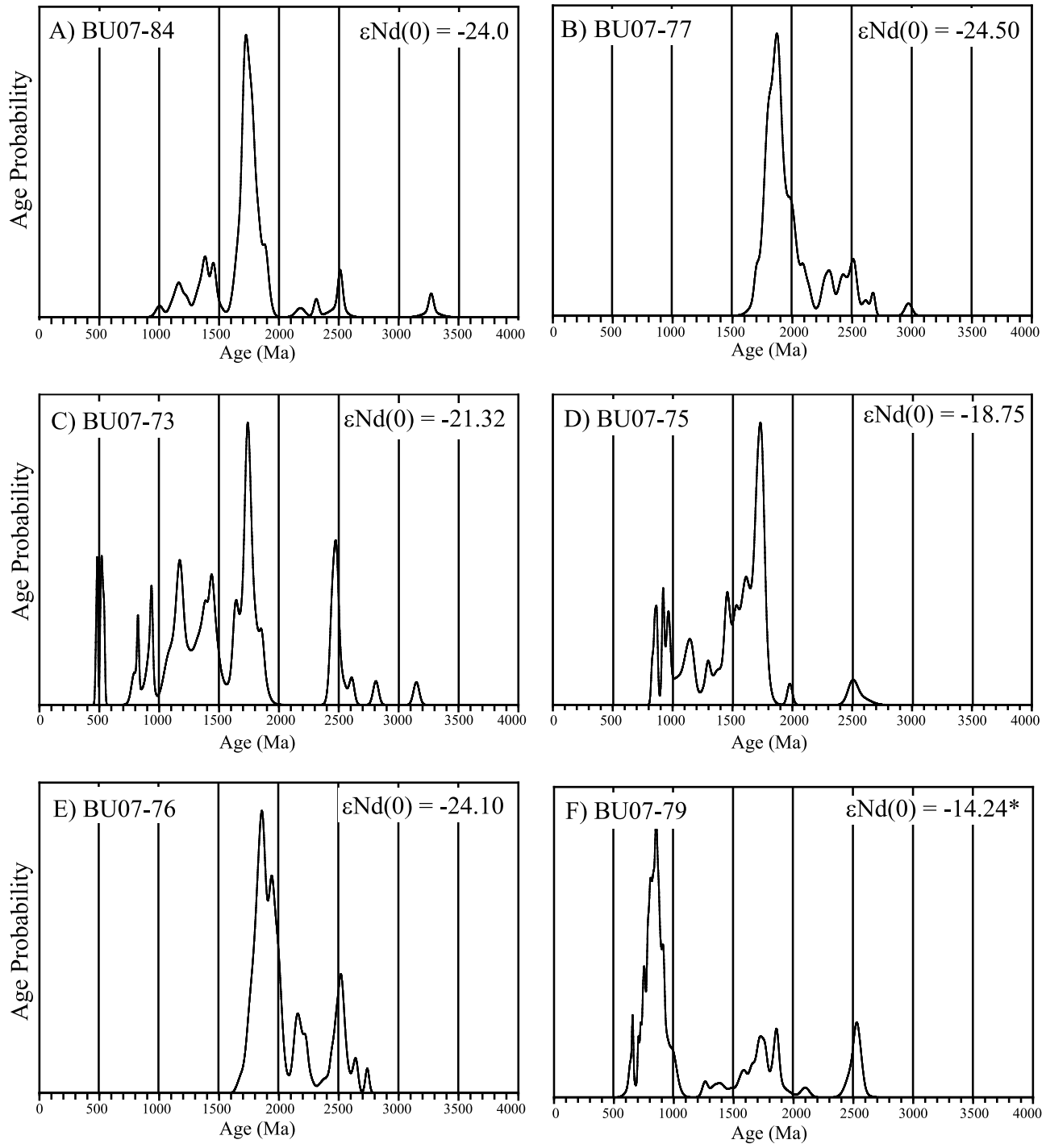

Figure 3b. Probability plots of samples A–F (see Figure 3a) showing U-Pb ages of detrital zircons.

measured Nd isotopic data (present-day values). Although the maximum and minimum depositional age, as well as the ages of potential source regions for LH and GH rocks can be inferred with varying degrees of confidence, they are essentially unknown for the Paro Formation. Thus rather than bias ε_{Nd} values with an assumed age for the source rock, we report Nd isotopic composition using $\varepsilon_{Nd}(0)$ values. This is a common practice for Himalayan rocks and facilitates

Table 1. Sample Locations for Western Bhutan

Sample	°N (dd.ddddd)	°E (dd.ddddd)	Analysis	Formation	Lithology
NBH-22	27.43297	89.64098	ε_{Nd}	Paro	Schist
BU07-84	27.42561	89.41311	DZ	Paro	Quartzite
BU07-77	27.45644	89.52264	DZ and ε_{Nd}	Paro	Quartzite
BU07-73	27.02925	89.58050	DZ and εNd	Paro	Quartzite
BU07-75	27.15200	89.54175	DZ and εNd	Paro	Quartzite
BU07-76	27.22606	89.51678	DZ and εNd	Paro	Quartzite
BU07-83	27.26186	89.35925	Zircon and εNd	Paro	Orthogneiss
BU07-79	27.33758	89.57497	DZ	Paro	Quartzite
BU08-128	27.33325	89.57353	Zircon	Paro	Orthogneiss

comparison with previous work in Bhutan and along the Himalayan arc.

5. Results

5.1. Field Mapping

5.1.1. Map View Description

[31] The Paro Formation crops out in a ~700 km^2 window in western Bhutan and contains metasedimentary rocks intruded by thin, 100–200 m sills of orthogneiss (Figure 2). Our mapping confirms that the Paro Formation is exposed as a tectonic window and that it is separated from the overlying GH section by a top-to-the-south thrust contact. Bedding in quartzite and marble and foliation in schist horizons dip north, south, east, and west at the northern, southern, eastern, and western edges, respectively, which defines a structural dome with the structurally deepest part exposed at Sisina (Figure 2).

[32] To the south of the main window, the Paro Formation is exposed again in a thrust sheet that is ~ 2.0 km wide (N-S) and ~50 km long (E-W) on the map with a structural thickness of ~1.5 km, bounded on both sides by north-dipping thrusts. Here the thrust and GH section overlying the Paro Formation has been folded into a synform between the northern and southern exposures of the Paro Formation. The southern boundary of the southern Paro Formation exposure is a north-dipping thrust fault that places the Paro Formation over GH rocks. On both sides of the fault, bedding planes and foliations are steeply north dipping (50°–56°) and are separated by a 2–3 m thick zone of gouge and altered rock. There is a sharp contrast in lithology with melt-bearing paragneiss in the footwall and quartzite with schist interbeds in the hanging wall. Asymmetric feldspar σ clasts and macroscopic fold vergence show a top-to-the-south shear sense. We interpret this contact as an out-of-sequence thrust (Figure 2) that placed the Paro Formation over GH rocks.

5.1.2. Stratigraphic Description

[33] Rocks of the Paro Formation can be divided into several thin (2 km to 100s of meters) but mappable units. We describe these units from the base of the Paro Formation to the top and argue that the relationships between the mapped units are stratigraphic. The base of the Paro Formation is a 600 m thick schist unit, which contains muscovite-biotite-garnet-staurolite-kyanite mineral assemblages. Kyanite is present within quartz veins, and rarely with biotite, but textures do not indicate the presence of any in situ partial melt. Also, within this schist unit is a two mica, granitic gneiss (~110 m thick) exposed on the either side of river at Sisina (Figures 2 and 3a).

[34] The schist unit is overlain by a gray colored, thin-bedded, fine-grained micaceous quartzite unit that is up to 1960 m thick (Figure 3a). The contact between the two units is gradational with thin quartzite layers within the schist becoming more prevalent and thicker upsection (Figure 4). Within the quartzite unit there are two marble bands. Marble band I is ~10 m thick and is stratigraphically lower, and marble band II is ~195 m thick and is stratigraphically higher. These two marble bands are recognized in seven different transects that extend across the Paro Formation and can be mapped as continuous bodies in the north (Haa, Chele La, Paro) and south (Chuzom, Betekha). The uniformity between the sections (Figure 3a) allows us to correlate the marble horizons around the full extent of the main window and emphasize a continuous stratigraphy through the Paro window (Figures 2 and 3a). Along the southwestern edge of the window, near Betekha and Shari are additional orthogneiss bodies. Near these intrusions are kyanite and fibrolite schist interbeds within the fine-grained micaceous quartzite unit (Figures 2 and 3a). Further upsection (Figure 2), we map small calc-silicate bodies associated with marble band III at Chele La, Tsaluna, and marble band II south of Thimphu (Figure 2).

Table 2. Epsilon Neodymium Isotopic Analyses

Sample	Sm (ppm)	Nd (ppm)	$^{143}Nd/^{144}Nd(0)$	Standard Error %	$\varepsilon_{Nd}(0)$	Formation	Lithology
NBH-22	6.62	24.86	0.511995	0.0016	−12.5	Paro	Schist
BU07-73	2.282	8.165	0.511545	0.0010	−21.3	Paro	Quartzite
BU07-75	7.552	28.970	0.511677	0.0009	−18.8	Paro	Quartzite
BU07-76	1.014	5.283	0.511402	0.0009	−24.1	Paro	Quartzite
BU07-77	0.848	3.235	0.511382	0.0008	−24.5	Paro	Quartzite
BU07-83	4.492	17.027	0.511978	0.0008	−12.9	Paro	Orthogneiss

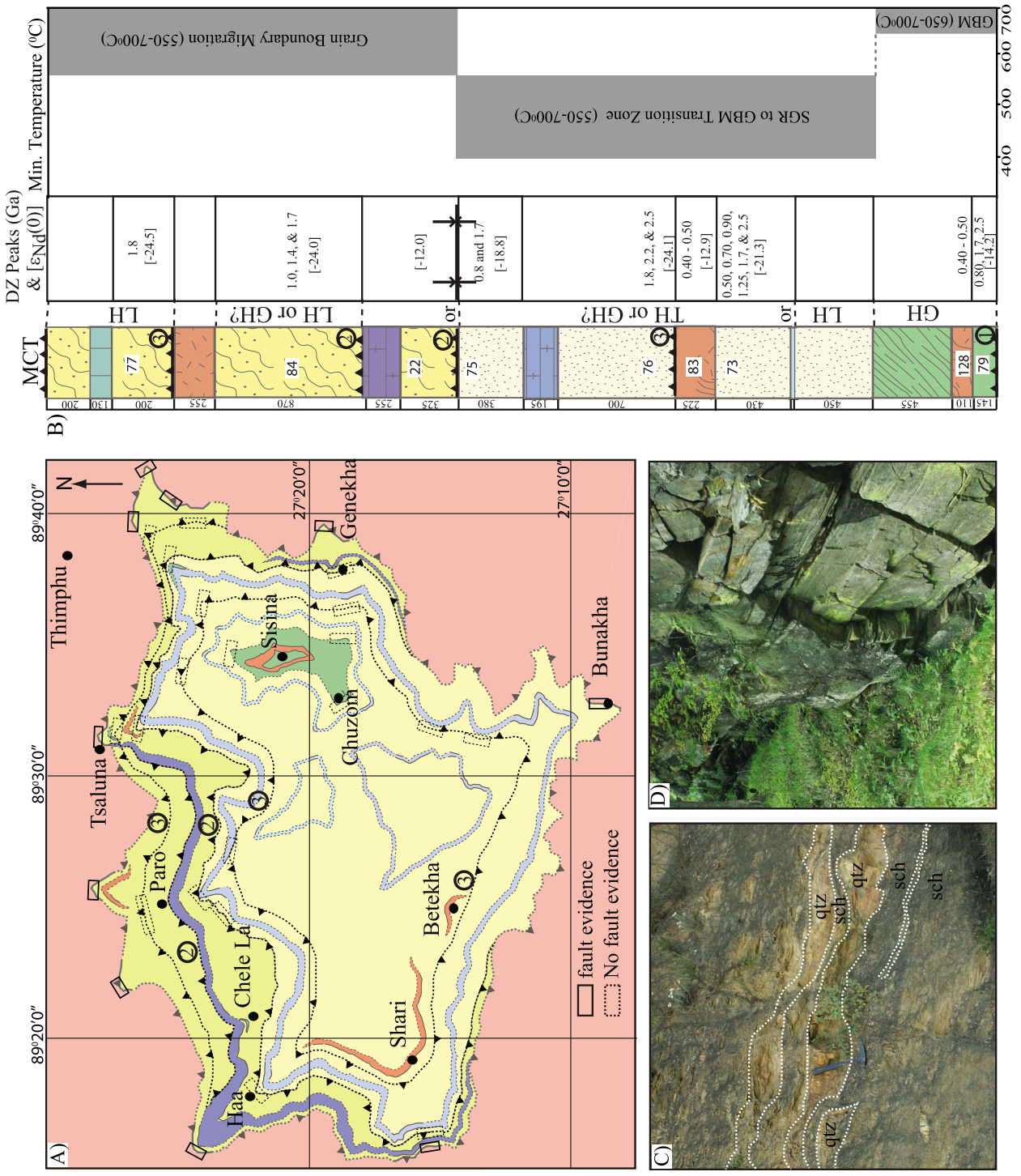
A)
Thimphu
Tsaluna
Paro
Haa
Chele La
Shari
Sisina
Chuzom
Genekha
Betekha
Bunakha
89°40'0"
89°30'0"
89°20'0"
27°20'0"
27°10'0"
N
fault evidence
No fault evidence
B)
MCT
DZ Peaks (Ga)
& [εNd(0)]
Min. Temperature (°C)
LH
LH or GH?
or
TH or GH?
LH
GH
1.8
[-24.5]
1.0, 1.4, & 1.7
[-24.0]
[-12.0]
0.8 and 1.7
[-18.8]
1.8, 2.2, & 2.5
[-24.1]
0.40 - 0.50
[-12.9]
0.50, 0.70, 0.90,
1.25, 1.7, & 2.5
[-21.3]
0.40 - 0.50
0.80, 1.7, 2.5
[-14.2]
Grain Boundary Migration (550-700°C)
SGR to GBM Transition Zone (550-700°C)
GBM (650-700°C)
400
500
600
700
C)
qtz
sch
D)

Figure 4

[35] Overlying the fine-grained quartzite unit is a tan-gray colored, coarse-grained, thin- to medium-bedded, biotite-rich quartzite unit, which is ~1600 m thick, and contains biotite-muscovite-garnet schist partings. The coarse-grained quartzite is beneath GH paragneiss at the eastern, western, and northern edges of Paro window (Figure 2). Within the coarse-grained quartzite of the Paro Formation is marble band III (~255 m thick) and two granite intrusions (~255 m thick), one just north of Paro and the other at Tsaluna (Figures 2 and 3a). Marble III is not exposed across the entire window and instead pinches out to the east, south of Genekha, and to the southwest of Betekha (Figure 2). Quartz microfabrics (amoeboid grains with large amplitude sutures and very large recrystallized grain sizes) associated with grain boundary migration recrystallization suggest the deformation temperatures of the coarse-grained quartzite are ~500°C–700°C, and the coarse-grained texture is a metamorphic fabric [*Stipp et al.*, 2002] (Figure 4). These high temperatures in the Paro Formation correlate with higher temperatures (> 700°) in the immediate hanging wall of the overlying thrust. The fine-grained quartzite in the south indicates temperatures of 400°C–500°C (associated with subgrain rotation recrystallization) and is overlain by cooler GH rocks whose peak temperature reached 600°C–≤ 700°C. In general, foliation is parallel to small (schist partings and interbeds) and large (first-order changes from schist to quartzite to marble) changes in lithology. We observe that foliation is parallel to the original sedimentary bedding throughout the Paro Formation, and that the planar (flattening) fabric is due to tectonic loading. Mesoscale folding is present in more incompetent lithologies, such as marble and interbeds of quartzite and schist. These are most prevalent at the base of Paro Formation near Chuzom, around the orthogneiss near Betekha and locally within marble band II (Figure 2). Folding is asymmetric and indicates top-to-the-south shear. The lack of foliation parallel to axial planes as well as lack of axial planar cleavage suggest that the development of foliation fabric parallel to bedding predates folding, that bedding orientations are right side up, and that the original, first-order stratigraphic succession is not repeated by isoclinal folding.

[36] In the southern exposure, the Paro Formation consists of metaquartzite and muscovite-biotite-garnet schist (Figure 2). This section is predominantly medium- to coarse-grained, micaceous quartzite (1500 m) overlain by interlayered fine-grained quartzite and schist above a thin band of marble (250 m) (Figure 2). The northern contact of the southern exposure is fine-grained quartzite overlain by GH paragneiss (muscovite-biotite-garnet-kyanite-fibrolite) containing partial melt textures. Based on the contact between the fine-grained quartzite and the overlying GH as well as the thickness of both the marble band and the underlying quartzite in the Paro Formation exposed in the south, we correlate the marble in the southern window with marble II in the northern window (Figure 3a).

[37] The stratigraphy we define above, schist overlain by fine-grained quartzite with marble bands I and II, overlain by coarse-grained quartzite with marble III, is recognized in each mapped transect across the Paro window. Because of this, stratigraphic sections drawn between Chuzom and Bunakha, Chuzom to Paro, Chuzom-Bemay Rong Chu, and Chuzom to Genekha are very similar except small, local variations in thickness (Figure 3a). In total, the average thickness of the Paro Formation in the Paro window is ~5.5 km, which is three times the exposed thickness of the fine-grained quartzite and marble band in the linear window further to the south (Figure 3a).

5.2. U-Pb Geochronology

[38] Sample BU07-79 is from quartzite interbedded within the staurolite-kyanite-schist unit at the base of the Paro Formation. This sample has a prominent youngest peak at 0.8 Ga with older, smaller peaks at 1.7 Ga and 2.5 Ga. BU08-128 is a granitic gneiss that is exposed at Sisina within the basal Paro Formation schist unit. Its likely age of crystallization is between 400 and 500 Ma (refer to Text S1, discussion 2 for further discussion).

[39] Four samples (BU07-73, BU07-75, BU07-76, and BU07-83) collected from the fine-grained quartzite unit were analyzed. Sample BU07-73 is from quartzite that we interpret as correlative to the fine-grained quartzite unit of the Paro Formation, from the southern exposure south of Chukha (Figure 2). It yielded a prominent peak at 1.7 Ga along with a series of smaller peaks at 0.50 Ga, 0.70 Ga, 0.90, 1.25 Ga, and 2.5 Ga (Figure 5). Sample BU07-76 which is stratigraphically above sample BU07-73 (based on correlating the marble in the southern exposure with marble II in the north), but in the main window, yielded a prominent peak centered at 1.8 Ga with two smaller and older peaks at 2.2 Ga and 2.5 Ga. Sample BU07-75 which is from the uppermost section of the fine-grained quartzite unit, has a strong peak at 1.7 Ga and a minor peak at 0.8 Ga. Sample BU07-83 is from an orthogneiss collected along the road to Haa near Shari (Figure 2). Similar to sample BU08-128, the likely crystallization age of this granite is between 400 to 500 Ma (refer to Text S1, discussion 2).

Figure 4. (a) Simplified geologic map of the Paro window with hypothetical faults (1, 2, and 3) drawn based on DZ and ε_{Nd} data. Solid and dashed rectangles are areas with and without evidence of fault, respectively. (b) Stratigraphic section of Paro Formation with hypothetical faults at various levels. Numbers 1, 2, and 3 correspond to permissible order of post MCT faulting if one assumes GH strata are north of LH strata [e.g., *DeCelles et al.*, 2000]. Note the boundary between fine- and coarse-grained quartzite can be either stratigraphic or the axis of a recumbent syncline that repeats lithological packages on both sides of axis (marble bands and orthogneiss), but the DZ and ε_{Nd} values do not match across limbs. Grey boxes to the right show temperature range of Paro Formation obtained from quartz deformation fabrics, i.e., subgrain rotation (SGR) (400°C–500°C), grain boundary migration (GBM) (500°C–700°C), and chessboard extinction (650°C –700°C) [*Stipp et al.*, 2002]. (c) Photo of gradational contact between schist (sch) and quartzite (qtz) near Sisina. (d) Photo of undeformed coarse-grained quartzite. Lithologic colors same as Figure 2.

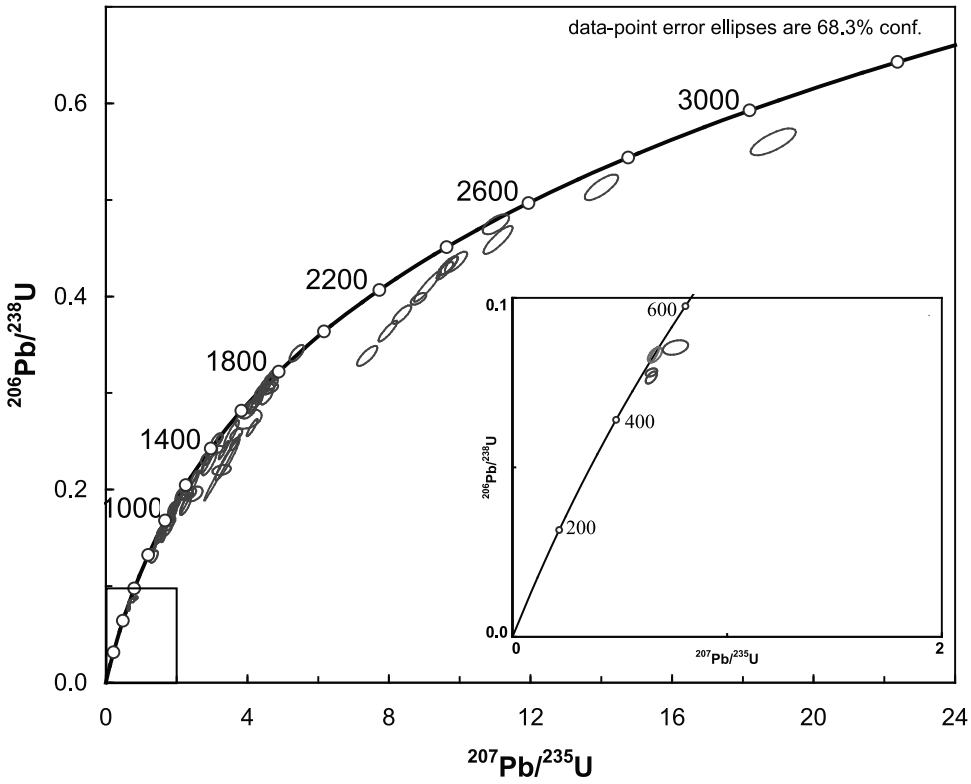

Figure 5. U-Pb concordia plot for 84 single zircon analyses of sample BU07-73 collected from the southern Paro Formation exposure south of Chukha, correlative to the base of the fine-grained quartzite unit of the Paro Window. This sample has a prominent peak at 1.7 Ga with a series of smaller peaks at 0.50 Ga, 0.70 Ga, 0.90, 1.25 Ga, and 2.5 Ga. The inset shows that two 500 Ma grains are not pulled off the concordia line and that the young peak is significant and robust. Error ellipses are shown at the 1σ level (68.3% confidence).

[40] Two samples (BU07-77, and BU07-84) collected from the coarse-grained quartzite unit were analyzed. Samples BU07-77 and BU07-84 are from the upper and lower parts of the section, respectively. BU07-77 has a strong peak at 1.8 Ga. Sample BU07-84 has a multiple-grain peak at ~1.7 Ga and smaller peaks at 1.0 Ga and 1.4 Ga.

[41] In addition, a sample from the JF (BU08-135) in western Bhutan was analyzed. DZ ages from this sample display a series of peaks between 475 Ma and 530 Ma, 1.0 Ga and 1.7 Ga, and a prominent peak at 2.5 Ga (Figure 6).

5.3. Epsilon Neodymium Isotope Geochemistry

[42] *McQuarrie et al.* [2008] reported ε_{Nd} values from four LH samples collected from eastern Bhutan, two from the Jaishidanda Formation, in the immediate footwall of the MCT, one from Baxa Formation, and one from the Diuri Formation. These samples have $\varepsilon_{Nd}(0)$ values of −19.4, −21.4, −21.4, and −19.8, respectively.

[43] *Richards et al.* [2006] reported $\varepsilon_{Nd}(500)$ values of 21 samples collected from the Bhutan Himalaya, out of which 6 were from LH rocks, 12 were from GH rocks, and 3 were from the Paro Formation. Here, we recalculate these as $\varepsilon_{Nd}(0)$ values. The six LH samples (one garnet schist, two quartzite and three phyllite samples) were from the Jaishidanda Formation and the Daling-Shumar Group south of the MCT. The five Daling-Shumar samples have an average $\varepsilon_{Nd}(0)$ value of −25.9 typical of the lower LH. Sample Bh12, located at the base of Jaishidanda Formation in western Bhutan, has an $\varepsilon_{Nd}(0)$ value of −16.6. The less negative value led *Richards et al.* [2006] to interpret this sample as part of the GH section. Three garnetiferous schist samples (B85, B88, and Bh10) sampled from the base of the Paro Formation (Figure 3a) have $\varepsilon_{Nd}(0)$ values of −14.2, 16.9, and 16.3.

[44] The predominantly old DZ ages that we obtained for most of our Paro Formation samples contrast strongly with the less negative ε_{Nd} values obtained by *Richards et al.* [2006]. To evaluate whether the Paro Formation has a mixture of old and young sources and to examine possible sediment sorting effects, we measured Sm and Nd isotopic ratios on the same samples we analyzed for U-Pb geochronology (i.e., BU07-73, 75, 76, 77, 83, and 84). In addition, we also collected one sample (NBH-22) (schist) at the same stratigraphic level as BU07-77 and BU07-84 (quartzite) to look at the isotopic signatures of sandstone-shale pairs.

[45] Sample BU07-76, collected from the lower section of the fine-grained quartzite, has an $\varepsilon_{Nd}(0)$ value of −24.1 (Figure 3a), while the garnetiferous schist at the same

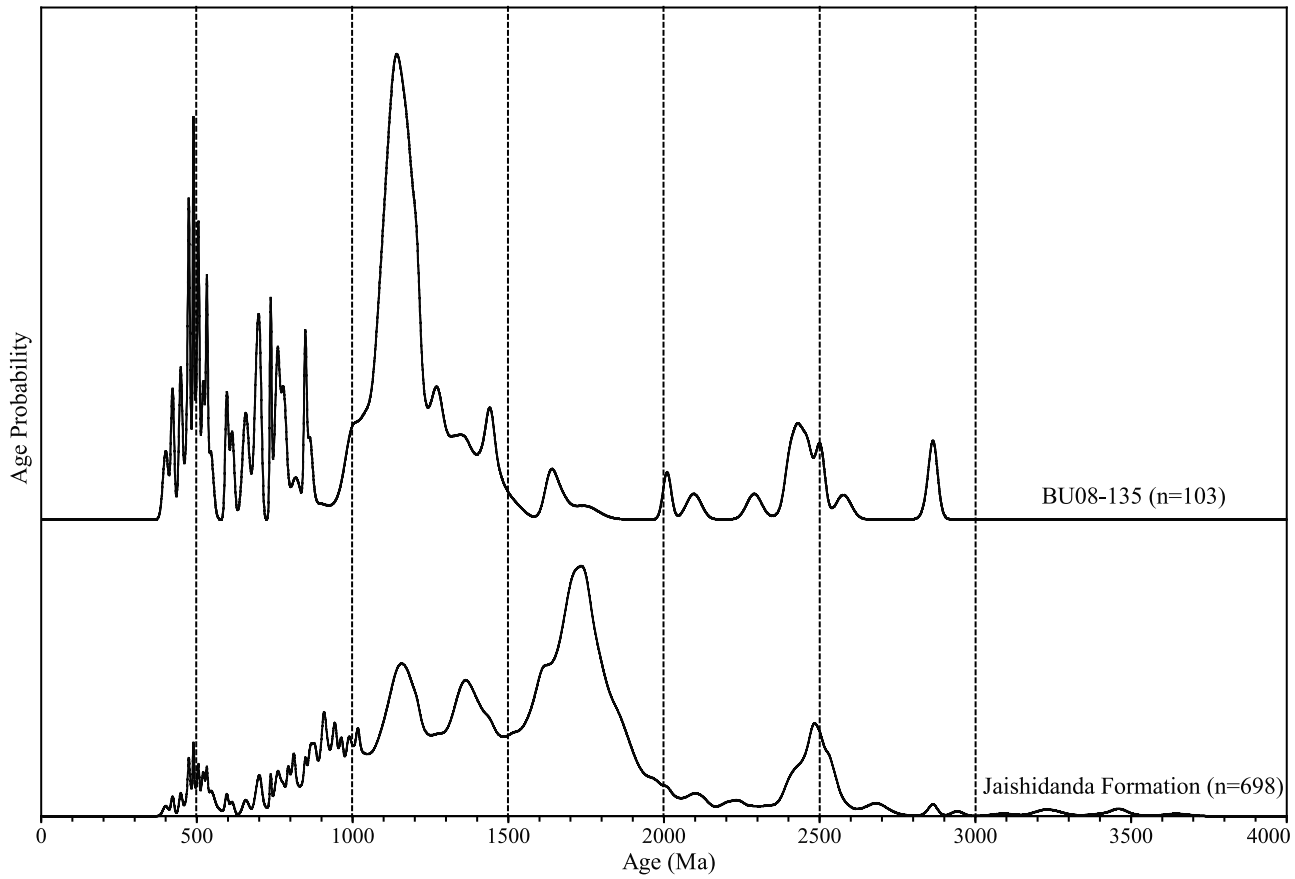

Figure 6. U-Pb detrital zircon age spectra of sample BU08-135 from western Bhutan and a composite U-Pb detrital zircon age spectra of Jaishidanda Formation (compiled from data presented in *McQuarrie et al.* [2008] and *Long et al.* [2010]) from eastern Bhutan displaying a series of peaks between 475 Ma and 530 Ma, 1.0 Ga and 1.7 Ga, and a prominent peak at 2.5 Ga. Refer to Figure 2 for sample locations. Sample Bh12 of *Richards et al.* [2006] collected from the same stratigraphic level as BU08-135 yield an $\varepsilon_{Nd}(0)$ value of −16.6.

stratigraphic level has $\varepsilon_{Nd}(0)$ value of −16.3 [*Richards et al.*, 2006]. Sample BU07-73 was also collected from the lower section of the fine-grained quartzite, but from the southern exposure, has an $\varepsilon_{Nd}(0)$ of −21.3 (Figure 3a). Sample BU07-75 collected from the upper section of the fine-grained quartzite has $\varepsilon_{Nd}(0)$ value of −18.8. The orthogneiss (BU07-83) within this quartzite unit has $\varepsilon_{Nd}(0)$ value of −12.9.

[46] A schist sample (NBH-22) adjacent to BU07-84 and BU07-77 was collected from the lower section of the coarse-grained unit and has an $\varepsilon_{Nd}(0)$ value of −12.5, while BU07-84 has an $\varepsilon_{Nd}(0)$ value of −24.0 (Figure 3a). Sample BU07-77, collected from the upper part of this coarse-grained quartzite unit has an $\varepsilon_{Nd}(0)$ value of −24.5.

6. Discussion

[47] With many previous studies claiming that GH and LH rocks in the Himalayas are distinguishable by distinct DZ signatures and isotopic composition, the U-Pb geochronologic and isotopic data from the Paro Formation presented in this study provides us with a unique opportunity to test these hypotheses. This study shows that the Paro Formation can be interpreted as either (1) a single sedimentary succession in the western Bhutan Himalaya that requires both old (typically associated with LH strata) and young (typically associated with GH or TH strata) detritus (Figure 7) or (2) a complex package of isoclinally folded and/or thrusted strata where the fingerprints of Himalayan strata (LH, GH, TH) are unique and have been tectonically interleaved (Figure 4).

6.1. Provenance and Age of the Paro Formation

[48] Schist within the Paro Formation shows less negative $\varepsilon_{Nd}(0)$ values typical of sediments derived from relatively young sources that are consistent with the young (500 Ma; refer to Figure S3) DZ peak obtained from the Paro Formation in the southern exposure and the Cambrian-Ordovician granitic gneiss within the Paro Formation (note the similarity between the $\varepsilon_{Nd}(0)$ value of the granite (−12.9) and the $\varepsilon_{Nd}(0)$ of the schists (−12.0 to −16.9)). However, several DZ samples spread throughout the Paro Formation display a

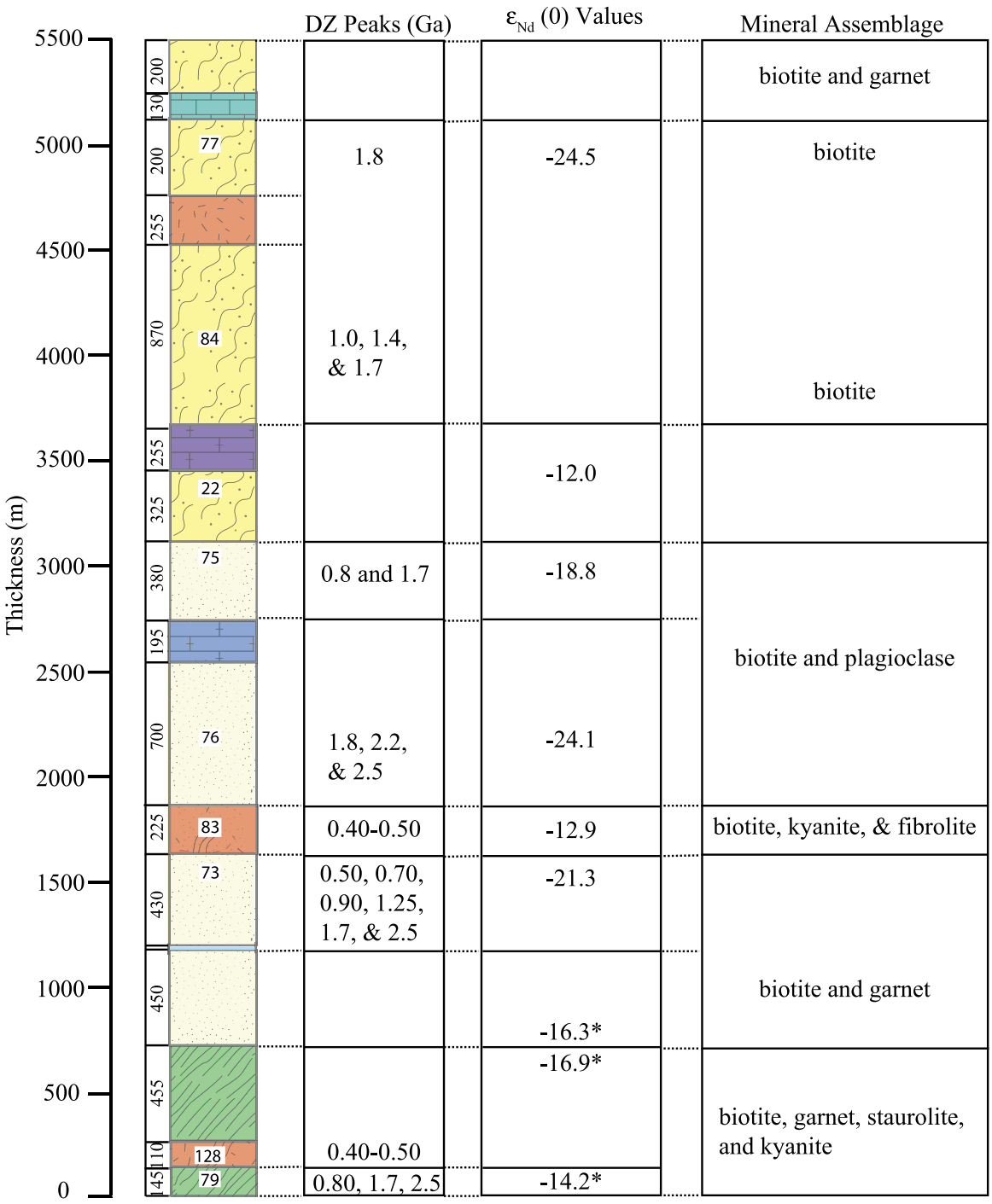

Figure 7. Composite stratigraphic section of the Paro Formation (~5.5 km thick) showing samples at various stratigraphic levels. Next to the section are detrital zircon peaks, ε_{Nd} values, and metamorphic mineral assemblages (bt, biotite; gar, garnet; plag, plagioclase; ky, kyanite; fib, fibrolite; st, staurolite). Both detrital zircon peaks and $\varepsilon_{Nd}(0)$ show no coherent pattern stratigraphically from low to high. Numbers with asteriks are $\varepsilon_{Nd}(0)$ values from *Richards et al.* [2006]. All samples have muscovite and quartz. Lithologic colors same as Figure 2.

significant peak at 1.8–1.9 Ga with minor young peaks (Figure 8) requiring that Paro Formation largely received sediment from very old sources. Assuming that the tectonostratigraphic zones throughout the Himalaya are distinguishable by the distinct DZ signatures and/or isotopic compositions described above (section 1), then using only the ε_{Nd} values obtained from schist, the Paro Formation would be correlated to the GH zone [*Richards et al.*, 2006]. However,

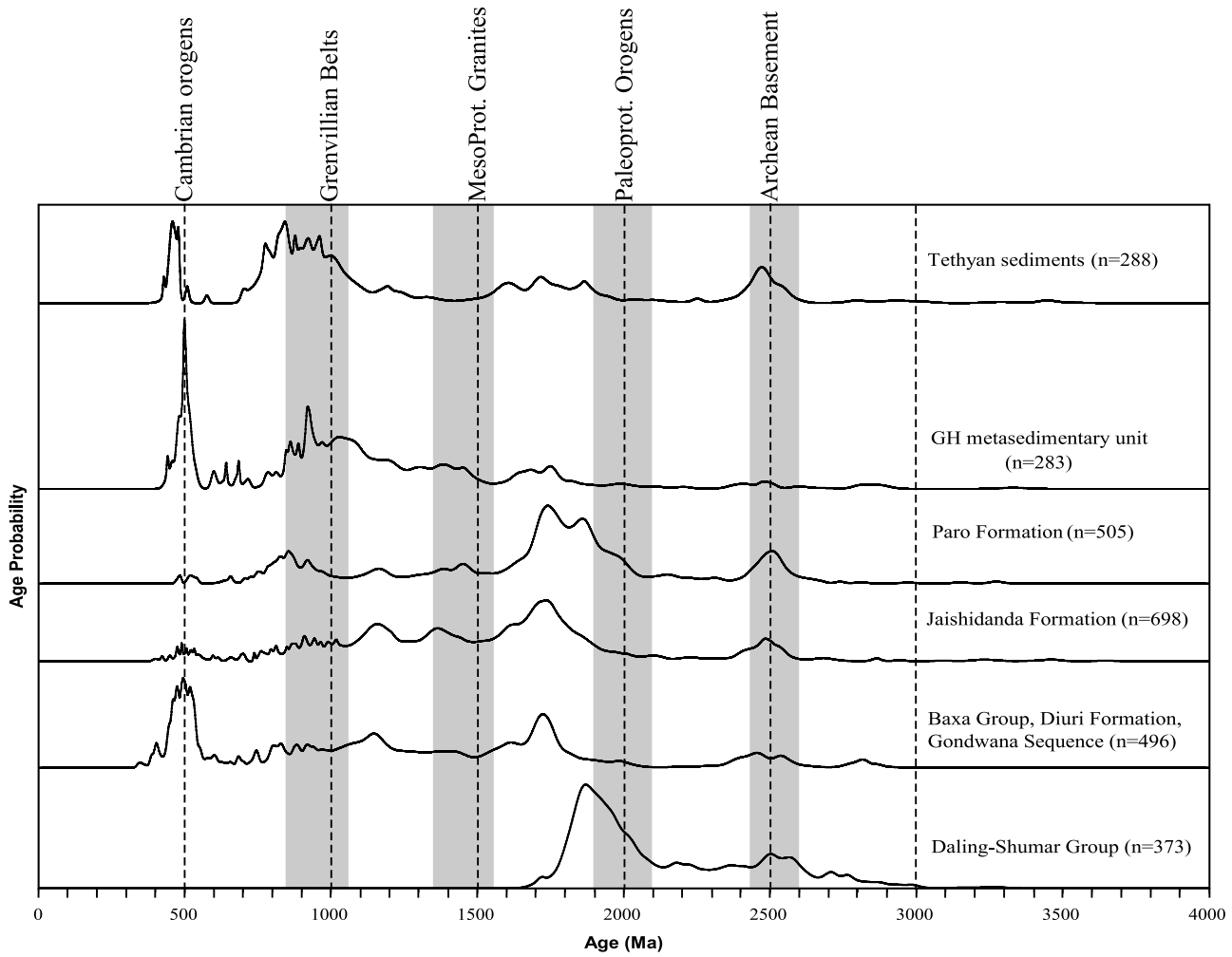

Figure 8. Composite U-Pb detrital zircon age spectra of all lithologic packages (Daling-Shumar Group, Paleozoic LH units, Jaishidanda Formation, Paro Formation, GH metasediments, and Tethyan sediments) in the Bhutan Himalaya. Other than data for the Paro Formation, all other data are compiled from *McQuarrie et al.* [2008], *Long and McQuarrie* [2010], and *Long et al.* [2010]. The number (n) beside each plot gives the total number of detrital zircon grains analyzed. Note the close resemblance of D2 spectra of the Paro Formation and the Jaishidanda Formation.

if our view of the Paro Formation was only from DZ samples BU07-76, 77, and 84 we would interpret the Paro Formation as Paleoproterozoic to Mesoproterozoic LH rocks. The presence of sediment ages that have previously been attributed to GH, LH and TH rocks within the Paro Formation lead us to propose that the Paro Formation received sediment from multiple source areas, both young and old. The combination of old DZs and less negative εNd values in the Paro Formation suggest that both LH and GH rocks are likely sources. Young Cambrian DZs from fine-grained quartzite sample BU07-73, which correlates to rocks in the immediate footwall of the MCT in the southern exposure, requires a Cambrian source. DZ spectra from the Bhutan Himalaya indicate that GH, TH and upper LH strata all contain Cambrian-Ordovician DZs with the exception of lower LH strata that only contain ≥1.8 Ga DZs [*McQuarrie et al.*, 2008; *Long and McQuarrie*, 2010; *Long et al.*, 2010]. In addition, the presence of 1.8 Ga DZs in the Paro Formation requires a 1.8 Ga source for grains with just 1.8 Ga zircons. Thus the Paro Formation could be completely sourced from upper LH rocks or the source rocks for LH strata, limiting a unique provenance interpretation.

[49] Arranging the Paro Formation as a single stratigraphic succession, and placing DZ and ε_{Nd} analyses in stratigraphic order (Figure 7) suggests that there is no coherent pattern in the age distribution of DZ and ε_{Nd} signatures. The DZ age signatures vary significantly within the stratigraphic section, suggesting that the Paro Formation was accumulated in a depositional setting characterized by abrupt changes in detrital input. This can result from a combination of active tectonics or a heterogeneous source region, as well as limited mixing of sediment within the basin [*DeGraaff-Surpless et al.*, 2003]. One possibility is the Paro Formation represents a basin caught between LH rocks on the northern

margin of India and GH rocks undergoing deformation [e.g., *Valdiya*, 1995; *Gehrels et al.*, 2003, 2006; *Cawood et al.*, 2007] to the north. Limited mixing is still required to explain the ε_{Nd} values. DZ ages and ε_{Nd} values analyzed on the same quartzite samples are consistent with each other while the ε_{Nd} values on schist are always significantly less negative, suggesting that the whole rock ε_{Nd} might have been affected by sedimentary sorting. Thus to determine the age spectrum that represents the entire Paro Formation requires combining the spectra from individual samples. A combination of several DZ spectra from a sedimentary succession creates a pattern that can be more confidently linked to source regions than any single spectrum [*Gehrels et al.*, 2000; *DeGraaff-Surpless et al.*, 2003].

[50] The youngest DZ peak in the Paro Formation exposed in the main window is 800 Ma, requiring the Paro Formation to be Neoproterozoic (~800 Ma) or younger in age. However, the presence of Cambrian (~500 Ma) DZs in the Paro Formation in the southern exposure as well as less negative $\varepsilon_{Nd}(0)$ values of schist in spite of at least one source of old sediment, suggests that the Paro Formation is possibly Cambrian or younger. We obtained an $\varepsilon_{Nd}(0)$ value of −12.9 on Silurian-Ordovician granite that intrudes the Paro Formation. Ashes (a highly labile component) from this (or slightly older Cambro-Ordovician magmatic events) could provide the young source material that is being preferentially concentrated in the schist of the Paro Formation [*McLennan et al.*, 1989]. The granite that intrudes the Paro Formation (BU08-128) limits the youngest deposition age at between 400 and 500 Ma.

6.2. Stratigraphic Section or Structural Repetition

[51] Because the Paro Formation is always in the footwall of a folded thrust that places GH rocks over either the Paro Formation or the Jaishidanda Formation, we suggest that this thrust is the MCT. Except for an abrupt transition in metamorphic grade, the rocks above and below the MCT in western Bhutan are broadly similar in composition. Schist of the GH and Paro Formation have similar ε_{Nd} values and they share all of the same DZ peaks, except for the presence of ~1.8–1.9 Ga peaks in the Paro Formation. Although the metamorphic grade of the Paro Formation is distinctly lower than the over riding GH rocks, most notably the presence of paragneiss with partial melt textures in the GH rocks [*Swapp and Hollister*, 1991; *Davidson et al.*, 1997], the garnet + biotite ± staurolite, kyanite and/or sillimanite metamorphic grade of the Paro Formation is similar to GH sections farther east in Bhutan [*Long and McQuarrie*, 2010]. The strongest argument for the thrust above the Paro window being the MCT is mapping that links the GH rocks above the Paro Formation to GH rocks in the south that are clearly in the hanging wall of the MCT (*Gansser* [1983]; *Bhargava* [1995]; our mapping).

[52] The structural setting of the Paro Formation, beneath the MCT may be used as an argument for structural repetition within the Paro Formation to explain varying DZ and ε_{Nd} signatures. Requiring a given DZ or ε_{Nd} signature to identify specific Himalayan units would require a complicated pattern of thrust faults and shear zones within the Paro window to explain geochronologic and geochemistry data. Figure 4 highlights the positions of hypothetical structures that could potentially interleave strata. Note that neither folds nor faults separate "matching" packages of rocks. In addition, our mapping argues against structural repetition, which is best shown by the contact between the lower schist unit and the fine-grained quartzite unit. At this boundary the change from schist to quartzite is gradational, with quartzite layers becoming more persistent upsection (Figure 4). There are no fault rocks or small-scale ductile structures (crenulations and shear bands) at this boundary. The same observations (no concentration of small-scale structures, faults, etc.) hold true for all of our hypothetical tectonic boundaries (Figure 4a). In addition, no change in metamorphic grade (with exception to the Betekha area which shows signs of contact metamorphism near an intrusive orthogneiss body) or strain gradient are observed. In contrast, the contact between the Paro Formation and the overlying GH rocks we map has highly altered and pervasively sheared rocks and boudinaged and folded quart veins in uppermost Paro Formation schist interbeds. These asymmetric boudins, C-S fabrics, and shear bands consistently show top-to-the-south shear sense. In addition, there is an abrupt change in metamorphic grade traversing from the upper part of Paro Formation to the lower section of GH paragneiss.

6.3. Provenance and Age of the Jashidanda Formation

[53] The combined DZ age spectra for the Jaishidanda Formation and Paro Formation, represented by 698 and 505 zircon grains, respectively, are almost identical (Figure 8). Both have prominent peaks at 1.25 Ga, 1.7 Ga, and 2.5 Ga, along with several zircons between 900 Ma and 480 Ma (Figure 8). While Mesoproterozoic-Neoproterozoic DZs could have the same sources as that of Paleozoic LH rocks, the Jaishidanda and Paro formations are unique in that they are the only strata that are directly below the MCT whose youngest DZ population is Cambro-Ordovician. Although there is nothing limiting the Jaishidanda Formation from being younger than Cambro-Ordovician, the presence of Silurian-Ordovician granite in the Paro Formation requires it to be older than ~400–500 Ma. We suggest that the source region for the young detritus in the Jaishidanda Formation and Paro Formation is the same as that proposed for similar age detritus in GH and TH rocks, which is from uplift and erosion of the GH section during the Cambro-Ordovician deformation and magmatic event that is recorded across the Himalaya [*Valdiya*, 1995; *Gehrels et al.*, 2003, 2006; *Cawood et al.*, 2007]. In addition to the similar DZ signature, both the Paro Formation and Jaishidanda Formation occupy the same structural level below the MCT. An important difference is thickness; the Paro Formation measures 5.5 km and the Jaishidanda Formation measures ~1.0 km.

7. Conclusions

[54] The use of DZ and ε_{Nd} signatures has been critical in defining lithotectonic units, aiding in deciphering the tectonic history in the central and western parts of the

Himalaya. However, new data from the western Bhutan Himalaya are in marked contrast to the increasingly accepted notion that different Himalayan tectonostratigraphic zones always have unique DZ and Nd isotopic signatures. Because these tectonostratigraphic zones record the precollisional geologic history of the Himalayas, the accurate reconstruction of their original depositional relationships is fundamentally important. Inaccuracies in correlations due to limited sampling of DZ spectra may have serious implications for the models of India-Asia collision.

[55] Our data show that DZ spectra may not be homogeneous within a given stratigraphic unit and that the youngest zircons do not necessarily represent the deposition age of the strata. Hence the necessity for multiple samples from the same unit to define variability and substantiate provenance conclusions as limited sampling potentially biases both provenance and tectonic interpretations.

[56] The Paro Formation in western Bhutan is a good example of a heterogeneous basin that contains both young (possibly sourced from the orogenesis preserved in GH rocks in the north) and old (from the Paleoproterozoic-Neoproterozoic sources in the south) material. In light of this new data we recommend caution in the use of DZ and ε_{Nd} signatures for tectonic interpretation especially when making correlations with studies that extend 1000s of km east or west of the original study sites.

[57] A strong detrital zircon signal at ~800 Ma implies that the Paro Formation must be Neoproterozoic in age, or younger. However, the presence of a ~500 Ma DZ peak in the southern exposure together with less negative $\varepsilon_{Nd}(0)$ values suggests that the Paro Formation is Cambrian or younger. Granite intrusion crystallization ages bracket the youngest permissible deposition age of the Paro Formation as Cambro-Ordovician.

[58] Because of the similarity in structural position and DZ age spectra, we correlate the Paro Formation with the Jaishidanda Formation, allowing us to align the formations (north to south, respectively) in reconstructing the precollisional Indian margin. Both these formations are recognized to occupy the same stratigraphic level (below the MCT). We suggest that the Paro and Jashidanda formations contain a detrital record of the Cambrian-Ordovician orogeny, which has not been previously recognized in LH rocks.

[59] **Acknowledgments.** We would like to thank Dorji Wangda (the former Director General), Department of Geology and Mines and Ugyen Wangda (Head), Geological Survey of Bhutan for their assistance and support. D. Robinson and D. Grujic are thanked for their insightful reviews. Victor Valencia and Alexander Pullen of the Arizona LaserChron Center (supported by EAR-0443387 and EAR-0732436) provided assistance with U-Pb dating. This work was supported by NSF EAR 0738522 to N. McQuarrie.

References

Ahmad, T., N. Harris, M. Bickle, H. Chapman, J. Bunbury, and C. Prince (2000), Isotopic constraints on the structural relationships between the Lesser Himalayan Series and the High Himalayan Crystalline Series, Garhwal Himalaya, *Geol. Soc. Am. Bull.*, *112*, 467–477, doi:10.1130/0016-7606(2000)112<467:ICOTSR>2.0.CO;2.

Argles, T., G. Foster, A. Whittington, N. Harris, and M. George (2003), Isotope studies reveal a complete Himalayan section in the Nanga Parbat syntaxis, *Geology*, *31*, 1109–1112, doi:10.1130/G19937.1.

Awwiller, D. N., and L. E. Mack (1989), Diagenetic resetting of Sm-Nd isotope systematics in Wilcox Group sandstones and shales, San Marcos Arch, south-central, Texas, *Trans. Gulf Coast Assoc. Geol. Soc.*, *39*, 321–330.

Barbeau, D., M. N. Ducea, G. E. Gehrels, and J. B. Saleeby (2005), Detrital-zircon U-Pb geochronology and the origin of Salinia, *Geol. Soc. Am. Bull.*, *117*, 466–481, doi:10.1130/B25496.1.

Bhargava, O. N. (Ed.) (1995), *The Bhutan Himalaya: A Geological Account*, *Spec. Publ. Ser., Geol. Surv. India*, 39, 1–245.

Bhattacharyya, K., and G. Mitra (2009), A new kinematic evolutionary model for the growth of a duplex—An example from the Rangit duplex, Sikkim Himalaya, India, *Gondwana Res.*, *16*, 697–715, doi:10.1016/j.gr.2009.07.006.

Boghossian, N. D., P. J. Patchett, G. M. Ross, and G. E. Gehrels (1996), Nd isotopes and the source of sediments in the miogeocline of the Canadian Cordillera, *J. Geol.*, *104*, 259–277, doi:10.1086/629824.

Brookfield, M. E. (1993), The Himalayan passive margin from Precambrian to Cretaceous times, Sediment, *Geol.*, *84*, 1–35, doi:10.1016/0037-0738(93)90042-4.

Cawood, P. A., M. R. W. Johnson, and A. A. Nemchin (2007), Early Paleozoic orogenesis along the Indian margin of Gondwana: Tectonic response to Gondwana assembly, *Earth Planet. Sci. Lett.*, *255*, 70–84, doi:10.1016/j.epsl.2006.12.006.

Daniel, C. G., L. S. Hollister, R. R. Parrish, and D. Grujic (2003), Exhumation of the main central thrust from lower crustal depths, eastern Bhutan Himalaya, *J. Metamorph. Geol.*, *21*, 317–334, doi:10.1046/j.1525-1314.2003.00445.x.

Dasgupta, S. (1995a), Shumar Formation, in *The Bhutan Himalaya: A Geological Account*, edited by O. N. Bhargava, *Spec. Publ. Ser., Geol. Surv. India*, *39*, 64–78.

Dasgupta, S. (1995b), Jaishidanda Formation, in *The Bhutan Himalaya: A Geological Account*, edited by O. N. Bhargava, *Spec. Publ. Ser., Geol. Surv. India*, *39*, 79–88.

Davidson, C., D. Grujic, L. S. Hollister, and S. M. Schmid (1997), Metamorphic reactions related to decompression and synkinematic intrusion of leucogranite, High Himalayan Crystallines, Bhutan, *J. Metamorph. Geol.*, *15*, 593–612, doi:10.1111/j.1525-1314.1997.00044.x.

DeCelles, P. G., G. E. Gehrels, J. Quade, P. A. Kapp, T. P. Ohja, and B. N. Upreti (1998), Neogene foreland basin deposits, erosional unroofing, and the kinematic history of the Himalayan fold-thrust belt, western Nepal, *Geol. Soc. Am. Bull.*, *110*, 2–21, doi:10.1130/0016-7606(1998)110<0002:NFBDEU>2.3.CO;2.

DeCelles, P. G., G. E. Gehrels, J. Quade, B. laReau, and M. Spurlin (2000), Tectonic implications of U-Pb zircon ages of the Himalayan orogenic belt in Nepal, *Science*, *288*, 497–499, doi:10.1126/science.288.5465.497.

DeCelles, P. G., D. M. Robinson, J. Quade, T. P. Ojha, C. N. Garzione, P. Copeland, and B. N. Upreti (2001), Stratigraphy, structure, and tectonic evolution of the Himalayan fold-thrust belt in western Nepal, *Tectonics*, *20*, 487–509, doi:10.1029/2000TC001226.

DeCelles, P. G., G. E. Gehrels, Y. Najman, A. J. Martin, A. Carter, and E. Garzanti (2004), Detrital geochronology and geochemistry of Cretaceous-Early Miocene strata of Nepal: Implications for timing and diachroneity of initial Himalayan orogenesis, *Earth Planet. Sci. Lett.*, *227*, 313–330, doi:10.1016/j.epsl.2004.08.019.

DeGraaff-Surpless, K., J. B. Mahoney, J. L. Wooden, and M. O. McWilliams (2003), Lithofacies control in detrital zircon provenance studies: Insights from the Cretaceous Methow basin, southern Canadian Cordillera, *Geol. Soc. Am. Bull.*, *115*, 899–915, doi:10.1130/B25267.1.

Dickinson, W. R., and G. E. Gehrels (2003), U-Pb ages of detrital zircons from Permain and Jurassic eolian sandstones of the Colorado Plateau, USA: Paleogeographic implications, *Sediment. Geol.*, *163*, 29–66, doi:10.1016/S0037-0738(03)00158-1.

Frost, C. D., and D. Winston (1987), Nd isotope systematics from coarse- and fine-grained sediments: Examples from the middle Proterozoic Belt-Purcell Supergroup, *J. Geol.*, *95*, 309–327, doi:10.1086/629132.

Gaetani, M., and E. Garzanti (1991), Multicyclic history of the northern India continental margin (northwestern Himalaya), *AAPG Bull.*, *75*, 1427–1446.

Gansser, A. (1964), Geology of the Himalayas, 289 pp., Wiley-Interscience, London.

Gansser, A. (1983), Geology of the Bhutan Himalaya, 181 pp., Birkhauser Verlag, Basel, Switzerland.

Garzanti, E. (1999), Stratigraphy and sedimentary history of the Nepal Tethys Himalaya passive margin, *J. Asian Earth Sci.*, *17*, 805–827, doi:10.1016/S1367-9120(99)00017-6.

Gehrels, G. E., M. J. Johnsson, and D. G. Howell (1999), Detrital zircon geochronology of the Adams argillite and nation river formation, east-central Alaska, USA, *J. Sediment. Res.*, *69*, 135–144.

Gehrels, G. E., W. R. Dickinson, B. C. D. Riley, S. C. Finney, and M. T. Smith (2000), Detrital zircon geochronology of the Roberts Mountains allochthon, Nevada, in *Paleozoic and Triassic Paleogeography and Tectonics of Western Nevada and Northern California*, edited by M. J. Soreghan and G. E. Gehrels, *Spec. Pap. Geol. Soc. Am.*, 347, 19–42.

Gehrels, G. E., P. G. DeCelles, A. Martin, T. P. Ojha, and G. Pinhassi (2003), Initiation of the Himalayan orogen as an early Paleozoic thin-skinned thrust belt, *GSA Today*, *13*, 4–9.

Gehrels, G. E., V. Valencia, and A. Pullen (2006), Detrital zircon geochronology by laser-ablation multicollector ICPMS at the Arizona LaserChron

Center, in *Geochronology: Emerging Opportunities, Paleontological Society Short Course, October 21, 2006, Philadelphia, PA*, edited by T. Olszewski and W. Huff, *Paleontol. Soc. Pap.*, 12, 1–10.

Gleason, J. D., P. J. Patchett, W. R. Dickinson, and J. Ruiz (1994), Nd isotopes link Ouachita turbidites to Appalachian sources, *Geology*, *22*, 347–350, doi:10.1130/0091-7613(1994)022<0347:NILOTT>2.3.CO;2.

Golani, P. R. (1995), Thimphu Group, in *The Bhutan Himalaya: A Geological Account*, edited by O. N. Bhargava, *Spec. Publ. Ser., Geol. Surv. India*, *39*, 89–108.

Grujic, D., L. S. Hollister, and R. R. Parrish (2002), Himalayan metamorphic sequence as an orogenic channel: Insight from Bhutan, *Earth Planet. Sci. Lett.*, *198*, 177–191, doi:10.1016/S0012-821X(02)00482-X.

Guha Sarkar, T. K. (1979), Geology of Geylegphug-Tongsa-Byakar area, central Bhutan, *Geol. Surv. India Misc. Publ.*, *4*(1), 359–374.

Heim, A., and A. Gansser (1939), Central Himalayas—Geological observations of Swiss expedition, 1936, *Mem. Soc. Hel. Sci. Nat.*, *73*, 1–245.

Hodges, K. V. (2000), Tectonics of the Himalayas and southern Tibet from two perspectives, *Geol. Soc. Am. Bull.*, *112*, 324–350, doi:10.1130/0016-7606(2000)112<324:TOTHAS>2.0.CO;2.

Hughes, N. C., P. M. Myrow, N. R. McKenzie, D. A. T. Harper, O. N. Bhargava, S. K. Tangri, K. S. Ghalley, and C. M. Fanning (2010), Cambrian rocks and faunas of the Wachi La, Black Mountains, Bhutan (online), *Geol. Mag.*, doi:10.1017/S0016756810000750.

Ikemoto, M. (2000), The Paro Formation in the Thimphu area, *Bhutan Geol.*, *3*, 5–7.

Imayama, T., and K. Arita (2008), Nd isotopic data reveal the material and tectonic nature of the Main Central Thrust zone in Nepal Himalaya, *Tectonophysics*, *451*(1–4), 265–281, doi:10.1016/j.tecto.2007.11.051.

Jangpangi, B. S. (1974), Stratigraphy and tectonics of parts of eastern Bhutan, Himal, *Geol.*, *4*, 117–136.

Jangpangi, B. S. (1978a), Stratigraphy and tectonics of parts of eastern Bhutan, *Himal. Geol.*, *4*, 117–136.

Jangpangi, B. S. (1978b), Stratigraphy and structure of Bhutan Himalaya, in Tectonic Geology of the Himalaya, edited by P. S. Saklani, pp. 221–242, Today'ass and Tomorrow's Publ., New Delhi.

Jangpangi, B. S. (1980), Lithostratigraphy and correlation of Daling (Phuntsholing), Buxa and Shumar formations of Bhutan Lesser Himalaya, in *Stratigraphy and Correlations of Lesser Himalayan Formations*, edited by K. S. Valdiya and S. B. Bhatia, pp. 211–222, Hindustan Publ., New Delhi.

Kellett, D. A., D. Grujic, and S. Erdmann (2009), Miocene structural reorganization of the South Tibetan detachment, eastern Himalaya: Implications for continental collision, *Lithosphere*, *1*(5), 259–281, doi:10.1130/L56.1.

Koike, T. (2002), Structural problem of the Paro Formation Southwestern Bhutan, *Bhutan Geology*, *6*, 10–18.

Lakshminarayana, G., and B. Singh (1995), Siwalik Group, in *The Bhutan Himalaya: A Geological Account*, edited by O. N. Bhargava, *Spec. Publ. Ser., Geol. Surv. India*, *39*, 23–28.

Le Fort, P. (1975), Himalayas: The collided range. Present knowledge of the continental arc, *Am. J. Sci.*, *275-A*, 1–44.

Long, S., and N. McQuarrie (2010), Placing limits on channel flow: Insights from the Bhutan Himalaya, *Earth Planet. Sci. Lett.*, *290*, 375–390, doi:10.1016/j.epsl.2009.12.033.

Long, S., N. McQuarrie, T. Tobgay, C. Rose, G. Gehrels, and D. Grujic (2010), Tectonostratigraphy of the Lesser Himalaya of Bhutan: Implications for the along-strike stratigraphic continuity of the northern Indian margin, *Geol. Soc. Am. Bull.*, doi:10.1130/B30202.1, in press.

Mapes, R. W. (2009), Past and present provenance of the Amazon, doctoral dissertation, *Dep. of Geol. Sci.*, Univ. of N. C. at Chapel Hill, Chapel Hill.

Martin, A. J., P. G. DeCelles, G. E. Gehrels, P. J. Patchett, and C. Isachsen (2005), Isotopic and structural constraints on the location of the Main Central Thrust in the Annupurna Range, central Nepal Himalaya, *Geol. Soc. Am. Bull.*, *117*, 926–944, doi:10.1130/B25646.1.

McCulloch, M. T., and G. J. Wasserburg (1978), Sm-Nd and Rb-Sr chronology of continental crust formation, *Science*, *200*, 1003–1011, doi:10.1126/science.200.4345.1003.

McLennan, S. M., M. T. McCulloch, S. R. Taylor, and J. B. Maynard (1989), Effects of sedimentary sorting on neodymium isotopes in deep-sea turbidites, *Nature*, *337*, 547–549, doi:10.1038/337547a0.

McLennan, S. M., S. R. Taylor, M. T. McCulloch, and J. B. Maynard (1990), Geochemical and Nd-Sr isotopic composition of deep-sea turbidites: Crustal evolution and plate tectonic associations, *Geochim. Cosmochim. Acta*, *54*, 2015–2050, doi:10.1016/0016-7037(90)90269-Q.

McQuarrie, N., D. Robinson, S. Long, T. Tobgay, D. Grujic, G. Gehrels, and M. Ducea (2008), Preliminary stratigraphic and structural architecture of Bhutan: Implications for the along-strike architecture of the Himalayan orogen, *Earth Planet. Sci. Lett.*, *272*, 105–117, doi:10.1016/j.epsl.2008.04.030.

Myrow, P. M., N. C. Hughes, T. S. Paulsen, I. S. Williams, S. K. Parcha, K. R. Thompson, S. A. Bowring, S.-C. Peng, and A. D. Ahluwalia (2003), Integrated tectonostratigraphic analysis of the Himalaya and implications for its tectonic reconstruction, *Earth Planet. Sci. Lett.*, *212*, 433–441, doi:10.1016/S0012-821X(03)00280-2.

Myrow, P. M., N. C. Hughes, M. P. Searle, C. M. Fanning, S.-C. Peng, and S. K. Parcha (2009), Stratigraphic correlation of Cambrian-Ordovician deposits along the Himalaya: Implications for the age and nature of rocks in the Mount Everest region, *Geol. Soc. Am. Bull.*, *121*, 323–332, doi:10.1130/B26384.1.

Myrow, P. M., N. C. Hughes, J. W. Goodge, C. M. Fanning, I. S. Williams, S. Peng, O. N. Bhargava, S. K. Parcha, and K. R. Pogue (2010), Extraordinary transport and mixing of sediment across Himalayan central Gondwana during the Cambrian-Ordovician, *Geol. Soc. A. Bull.*, *122*, 1660–1670.

Nesbitt, H. W., and G. M. Young (1996), Petrogenesis of sediments in the absence of chemical weathering: Effects of abrasion and sorting on bulk composition and mineralogy, *Sedimentology*, *43*, 341–358, doi:10.1046/j.1365-3091.1996.d01-12.x.

Ohr, M., A. N. Halliday, and D. R. Peacor (1991), Sr and Nd evidence for punctuated diagenesis, Texas Gulf Coast, *Earth Planet. Sci. Lett.*, *105*, 110–126, doi:10.1016/0012-821X(91)90124-Z.

Otamendi, J. E., M. N. Ducea, A. M. Tibaldi, G. W. Bergantz, J. D. de la Rosa, and G. I. Vujovich (2009), Generation of tonalitic and dioritic magmas by coupled partial melting of gabbroic and metasedimentary rocks within the deep crust of the Famatinian magmatic arc, Argentina, *J. Petrol.*, *50*, 841–873, doi:10.1093/petrology/egp022.

Parrish, R. R., and K. V. Hodges (1996), Isotopic constraints on the age and provenance of the Lesser and Greater Himalayan sequences, Nepalese Himalaya, *Geol. Soc. Am. Bull.*, *108*, 904–911, doi:10.1130/0016-7606(1996)108<0904:ICOTAA>2.3.CO;2.

Potter, P. E., Y. Huh, and J. M. Edmond (2001), Deep-freeze petrology of Lena River sand, Siberia, *Geology*, *29*, 999–1002.

Quade, J., J. M. L. Cater, T. P. Ohja, J. Adam, and T. M. Harrison (1995), Late Miocene environmental change in Nepal and the northern Indian subcontinent: Stable isotope evidence from paleosols, *Geol. Soc. Am. Bull.*, *107*, 1381–1397, doi:10.1130/0016-7606(1995)107<1381:LMECIN>2.3.CO;2.

Ray, S. K., B. K. Bandyopadhyay, and R. K. Razdan (1989), Tectonics of a part of the Shumar allochthon in eastern Bhutan, *Tectonophysics*, *169*, 51–58, doi:10.1016/0040-1951(89)90182-0.

Richards, A., T. Argles, N. Harris, R. Parrish, T. Ahmad, F. Darbyshire, and E. Draganits (2005), Himalayan architecture constrained by isotopic tracers from clastic sediments, *Earth Planet. Sci. Lett.*, *236*, 773–796, doi:10.1016/j.epsl.2005.05.034.

Richards, A., R. Rarrish, N. Harris, T. Argles, and L. Zhang (2006), Correlation of lithotectonic units across the eastern Himalaya, Bhutan, *Geology*, *34*, 341–344, doi:10.1130/G22169.1.

Robinson, D. M., P. G. DeCelles, P. J. Patchett, and C. N. Garzione (2001), The kinematic evolution of the Nepalese Himalaya interpreted from Nd isotopes, *Earth Planet. Sci. Lett.*, *192*, 507–521, doi:10.1016/S0012-821X(01)00451-4.

Robinson, D., P. G. DeCelles, and P. Copeland (2006), Tectonic evolution of the Himalayan thrust belt in western Nepal: Implications for channel flow models, *Geol. Soc. Am. Bull.*, *118*, 865–885, doi:10.1130/B25911.1.

Savage, K. M., and P. E. Potter (1991), Petrology of modern sands of the Rios Guaviare and Inirida, southern Columbia; tropical climate and sand composition, *J. Geol.*, *99*, 289–298, doi:10.1086/629489.

Segupta, S., and P. L. Raina (1978), Geology of parts of the Bhutan foothills adjacent to Darjeeling district, Indian *J. Earth Sci.*, *5*(1), 20–23.

Sircombe, K. N. (1999), Tracing provenance through the isotope ages of littoral and sedimentary detrital zircon, eastern Australia, *Sediment. Geol.*, *124*, 47–67, doi:10.1016/S0037-0738(98)00120-1.

Sircombe, K. N., and M. L. Hazelton (2004), Comparison of detrital zircon age distributions by kernel functional estimation, *Sediment. Geol.*, *171*, 91–111, doi:10.1016/j.sedgeo.2004.05.012.

Stipp, M., H. Stunitz, R. Heilbronner, and S. M. Schmid (2002), The eastern Tonale fault zone: A "natural laboratory" for crystal plastic deformation of quartz over a temperature range from 250° to 700°C, *J. Struct. Geol.*, *24*, 1861–1884, doi:10.1016/S0191-8141(02)00035-4.

Swapp, S. M., and L. S. Hollister (1991), Inverted metamorphism within the Tibetan slab of Bhutan: Evidence for a tectonically transported heat-source, Can, *Mineral.*, *29*, 1019–1041.

Tangri, S. K. (1995), Baxa Group, in *The Bhutan Himalaya: A Geological Account*, edited by O. N. Bhargava, *Spec. Publ. Ser., Geol. Surv. India*, *39*, 38–58.

Tangri, S. K., and A. C. Pande (1995), Tethyan sequence, in *The Bhutan Himalaya: A Geological Account*, edited by O. N. Bhargava, *Spec. Publ. Ser., Geol. Surv. India*, *39*, 109–141.

Trichal, A. K., and S. Jarayam (1989), Tungsten mineralization in skarn rocks, Dholpani-Bhurkhola areas, Geylegphug district, Bhutan, *Spec. Publ. Ser., Geol. Surv. India*, *22*, 101–105.

Upreti, B. N. (1999), An overview of the stratigraphy and tectonics of the Nepal Himalaya, *J. Asian Earth Sci.*, *17*, 577–606, doi:10.1016/S1367-9120(99)00047-4.

Valdiya, K. S. (1995), Proterozoic sedimentation and Pan-African geodynamic development in the Himalaya, *Precambrian Res.*, *74*, p. 35–55.

Whittington, A., G. Foster, N. Harris, D. Vance, and M. Ayres (1999), Lithostratigraphic correlations in the western Himalaya—An isotopic approach, *Geology*, *27*, 585–588, doi:10.1130/0091-7613(1999)027<0585:LCITWH>2.3.CO;2.

Yin, A. (2006), Cenozoic tectonic evolution of the Himalayan orogen as constrained by along-strike variation of structural geometry, exhumation history, and foreland sedimentation, *Earth Sci. Rev.*, *76*, 1–131, doi:10.1016/j.earscirev.2005.05.004.

Yin, A., C. S. Dubey, T. K. Kelty, A. A. G. Webb, T. M. Harrison, C. Y. Chou, and J. Celerier (2010), Geologic correlation of the Himalayan orogen and Indian craton: Part 2. Structural geology, geochronology and tectonic evolution of the eastern Himalaya, *Geol. Soc. Am. Bull.*, *122*(3–4), 360–395, doi:10.1130/B26461.1.

M. N. Ducea and G. Gehrels, Department of Geosciences, University of Arizona, 1040 East Fourth St., Tucson, AZ 85721, USA.

S. Long, N. McQuarrie, and T. Tobgay, Department of Geosciences, Princeton University, 208 Guyot Hall, Princeton, NJ 08544, USA. (ttobgay@princeton.edu)